1. REPORT DATE (DD-MM-YYYY) 06 July 2016	2. REPORT TYPE Journal Article	3. DATES COVERED (From - To) 21 April 2016 - 06 July 2016
4. TITLE AND SUBTITLE Organic Crystal Engineering of Thermosetting Cyanate Ester Monomers: Influence of Structure on Melting Point		5a. CONTRACT NUMBER
		5b. GRANT NUMBER
		5c. PROGRAM ELEMENT NUMBER
6. AUTHOR(S) Andrew J. Guenthner, Sean M. Ramirez, Michael D. Ford, Denisse Soto, Jerry A. Boatz, Kamran B. Ghiassi and Joseph M. Mabry		5d. PROJECT NUMBER
		5e. TASK NUMBER
		5f. WORK UNIT NUMBER Q16J
7. PERFORMING ORGANIZATION NAME(S) AND ADDRESS(ES) Air Force Research Laboratory (AFMC) AFRL/RQRP 10 E. Saturn Blvd. Edwards AFB, CA 93524-7680		8. PERFORMING ORGANIZATION REPORT NO.
9. SPONSORING / MONITORING AGENCY NAME(S) AND ADDRESS(ES) Air Force Research Laboratory (AFMC) AFRL/RQR 5 Pollux Drive Edwards AFB, CA 93524-7048		10. SPONSOR/MONITOR'S ACRONYM(S)
		11. SPONSOR/MONITOR'S REPORT NUMBER(S) AFRL-RQ-ED-JA-2016-139

12. DISTRIBUTION / AVAILABILITY STATEMENT
Approved for Public Release; Distribution Unlimited. PA Case Number: #16305; Clearance Date: 16 June 2016

14. ABSTRACT
Key principles needed for the rational design of thermosetting monomer crystals, in order to control the melting point, have been elucidated using both theoretical and experimental investigations of cyanate esters. A determination of the thermodynamic properties associated with melting showed that the substitution of silicon for the central quaternary carbon in the di(cyanate ester), 2,2-bis(4-cyanatophenyl)propane, resulted in an increase in the entropy of melting along with a decrease in the enthalpy of melting, leading to a decrease in the melting temperature of 21.8 ± 0.2 K. In contrast, the analogous silicon substitution in the tri(cyanate ester), 1,1,1-tris(4- cyanatophenyl)ethane, resulted in no significant changes to the enthalpy and entropy of melting, accompanied by a small increase of 1.5 ± 0.3 K in the melting point. The crystal structure of 1,1,1- tris(4-cyanatophenyl)ethane was determined via single crystal X-ray diffraction, and the structures of these four di(cyanate esters) and tri(cyanate esters) were examined. Although both the empirical models of Lian and Yalkowsky, as well as Chickos and Acree, provided reasonable estimates of the entropy of melting of 2,2-bis(4-cyanatophenyl)propane, they successfully predicted only certain effects of silicon substitution, and did not capture the difference in behavior between the di(cyanate esters) and the tri(cyanate esters). Semi-empirical molecular modeling, however, helped to validate an explanation of the mechanism for the increase in the entropy of melting of the silicon-containing di(cyanate ester), while providing insight into the reason for the difference in behavior between the di(cyanate esters) and tri(cyanate esters). Taken together, the results assist in understanding how freedom of molecular motions in the liquid state may control the entropy of melting, and can be utilized to guide the development of compounds with optimal melting characteristics for high-performance applications.

15. SUBJECT TERMS
thermosetting resin; thermosetting network; cyanate ester; monomer; crystal engineering; differential scanning calorimetry, X-ray diffraction

16. SECURITY CLASSIFICATION OF:			17. LIMITATION OF ABSTRACT	18. NUMBER OF PAGES	19a. NAME OF RESPONSIBLE PERSON A Guenthner
a. REPORT Unclassified	b. ABSTRACT Unclassified	c. THIS PAGE Unclassified	SAR	58	19b. TELEPHONE NO (include area code) N/A

Organic Crystal Engineering of Thermosetting Cyanate Ester Monomers: Influence of Structure on Melting Point

Andrew J. Guenthner*[1], Sean M. Ramirez[2], Michael D. Ford[2], Denisse Soto[3], Jerry A. Boatz[1], Kamran B. Ghiassi[1], and Joseph M. Mabry[1]

[1]Air Force Research Laboratory, Propulsion Directorate, Edwards AFB, CA 93524

[2]ERC Incorporated, Edwards AFB, CA 93524

[3]Naval Surface Warfare Center Indian Head EOD Technology Division, Indian Head, MD 20640

Author e-mail: andrew.guenthner@us.af.mil

Keywords: thermosetting resin; thermosetting network; cyanate ester; monomer; crystal engineering; differential scanning calorimetry, X-ray diffraction

ABSTRACT

Key principles needed for the rational design of thermosetting monomer crystals, in order to control the melting point, have been elucidated using both theoretical and experimental investigations of cyanate esters. A determination of the thermodynamic properties associated with melting showed that the substitution of silicon for the central quaternary carbon in the di(cyanate ester), 2,2-bis(4-cyanatophenyl)propane, resulted in an increase in the entropy of melting along with a decrease in the enthalpy of melting, leading to a decrease in the melting temperature of 21.8 ± 0.2 K. In contrast, the analogous silicon substitution in the tri(cyanate ester), 1,1,1-tris(4-cyanatophenyl)ethane, resulted in no significant changes to the enthalpy and entropy of melting,

accompanied by a small increase of 1.5 ± 0.3 K in the melting point. The crystal structure of 1,1,1-tris(4-cyanatophenyl)ethane was determined via single crystal X-ray diffraction, and the structures of these four di(cyanate esters) and tri(cyanate esters) were examined. Although both the empirical models of Lian and Yalkowsky, as well as Chickos and Acree, provided reasonable estimates of the entropy of melting of 2,2-bis(4-cyanatophenyl)propane, they successfully predicted only certain effects of silicon substitution, and did not capture the difference in behavior between the di(cyanate esters) and the tri(cyanate esters). Semi-empirical molecular modeling, however, helped to validate an explanation of the mechanism for the increase in the entropy of melting of the silicon-containing di(cyanate ester), while providing insight into the reason for the difference in behavior between the di(cyanate esters) and tri(cyanate esters). Taken together, the results assist in understanding how freedom of molecular motions in the liquid state may control the entropy of melting, and can be utilized to guide the development of compounds with optimal melting characteristics for high-performance applications.

INTRODUCTION

Although not often discussed in the field of thermosetting materials, crystal engineering[1-4] plays a key role in facilitating the successful utilization of these substances for many high-performance applications. The class of thermosetting monomers known as cyanate esters,[5-8] for instance, are prized not only for the outstanding heat and fire resistance of the resultant networks, but also for their relatively low melting points, which enable affordable fiber-reinforced polymer composite formation processes such as filament winding and resin transfer molding to be utilized in the manufacturing high-performance cyanate ester products. The ability to combine high performance with affordable manufacturing is a distinct advantage of cyanate esters compared to

other classes of thermosetting monomers, and, in combination with other key properties such as outstanding resistance to high-energy radiation and very low hygrothermal expansion and volatile generation, enables them to find uses in highly demanding applications such as magnet encapsulants for thermonuclear fusion reactors[9,10] and structural components for interplanetary space probes.[11] Cyanate esters cure via an autocatalytic cyclotrimerization, with the process initiated either by adventitious impurities such as ambient water, or by intentionally-added catalysts. Although the precise mechanisms depend upon the method of initiation and catalyst type employed, the reaction pathways tend to converge on the highly stable cyanurate ring as the final product. Consequently, the cross-linked structure is almost entirely composed of repeating units linked together via triply-substituted cyanurate rings, and the reaction tends to be highly exothermic. These features enable monomers to begin to cure very rapidly after only a brief exposure to elevated temperatures.

The key feature to be controlled in crystals of cyanate ester monomers (as with all other thermosetting monomers) is the melting point. Because the monomer must be in the molten state at the start of fabrication operations, a high melting point (generally above 400 K) makes it difficult to handle the monomer in an operating environment that is open to ambient conditions (as is typical for filament winding, for instance) without partial crystallization. In typical operations that involve highly catalyzed samples, an elevated melting temperature also makes it difficult to melt and mix the monomer without initiating unwanted polymerization. Even a melting point above ~350 K imposes modest difficulties in melting, de-gassing, and mixing monomers and catalysts. Strategies such as oligomerization (creating a range of molecules with different molecular weights),[12,13] the use of multiple stereoisomers,[14] and simple mixing of miscible monomers[15-20] have been used to retard crystallization and/or lower melting points effectively. However, these strategies involve

drawbacks such as increased viscosity and difficulties in purification, as well as decreased storability and "out time" due to the comparative ease with which moisture infiltrates liquids, leading to side reactions. The ideal cyanate ester monomer can be readily crystallized for storage in the solid state, with a melting point modestly above ambient temperatures. In order to achieve this ideal property, the melting point must therefore be controlled carefully so as to fall in a relatively narrow range (315 - 340 K).

In a traditional approach to crystal engineering, the melting point could be adjusted by altering the network of interactions among functional groups in the crystal, thereby changing the enthalpy of melting, with concomitant changes to the entropy of melting. For reactive monomers, however, functional groups may not be altered in the crystal without significantly altering the properties of cure as well as the final polymerized networks. In addition, changes to the size, shape, and internal atomic connectivity in the monomers must also be carefully constrained so as not to alter the desirable properties of the polymerized networks. Fortunately, the field of crystal engineering provides examples where even very modest changes in the chemical structure of a molecule can induce significant changes in crystal melting properties.[21-24] In order to control melting temperatures, the changes can either lead to rearrangements of crystal packing (thereby primarily affecting the enthalpy of melting), or to changes in the internal motions available in the molten state (primarily affecting the entropy of melting). While the former approach is more common in crystal engineering, in this paper we show that the latter approach (which relies on the fact that the motions of large, rigid molecules in the melt are still constrained) may also be utilized to understand and control the melting points of monomeric crystals.

In order to demonstrate that entropic effects are significant, in addition to the fact that subtle changes in structure can exert a disproportionate influence on these effects, we combine

newly obtained, high-precision experimental data on four structurally-similar cyanate ester monomers with both empirical methods for estimating the thermodynamic properties of melting and semi-empirical molecular modeling approaches. Although numerous empirical approaches for predicting thermodynamic melting properties have been developed, we rely on two of the most recent and highly developed approaches by Lian and Yalkowsky[25] and by Chickos and Acree.[26] For molecular modeling, methods ranging from atomistic simulations with semi-empirical force fields to density functional theory methods were investigated in order to analyze the available motions of molecules in isolation. We demonstrate that the substitution of slightly longer Si-C bonds for C-C bonds in the monomer chemical structure results in the "unlocking" of new degrees of freedom in non-interlocking molecules, thereby increasing the entropy of melting and lowering the melting point. These results provide a detailed explanation as to why the substitution of Si for C lowers the melting point in certain types of cyanate ester monomers, while having no effect in others. Such detailed knowledge provides a basis for further development and optimization of the key properties of not only cyanate ester monomers, but of thermosetting molecules in general.

EXPERIMENTAL

Materials. The dicyanate ester of Bisphenol A, 2,2'-(4-cyanatophenyl)propane, available commercially as Primaset® BADCy, was obtained from Lonza. This dicyanate is one of the most widely studied, and the sample in our laboratory was consistent with the previously reported melting point of 356.0 ± 0.2 K, heat of fusion of 100 ± 9 J/g, and purity of 99.2 - 99.4%.[27] These results are in general agreement with other studies.[5,16-20,28-34] The silicon-containing analog of BADCy, bis(4-cyanatophenyl)dimethylsilane, or SiMCy, was synthesized in our laboratory according to a previously published procedure[27] that closely follows the original synthesis reported

5

by Wright.[28,35] SiMCy exhibits a previously reported melting point of 338.2 ± 0.1 K, heat of fusion of 93 ± 1 J/g, and purity of 99.4 ± 0.1% after purification using chromatography.[27] The tricyanate analog of BADCy, 1,1,1-tris(4-cyanatophenyl)ethane, known by the trade name ESR-255, and was originally synthesized by Hi-Tek polymers.[36] The material used for analysis was synthesized and kindly provided by Dr. Matthew Davis at the Naval Air Warfare Center.[37] The ESR-255 sample was consistent with the reported melting point of 388.5 ± 0.3K, heat of melting of 72 ± 4 J/g, and purity of 99.4 ± 0.2%.[27] The silicon-containing analog of ESR-255, tris(4-cyanatophenyl)methylsilane, also known as SiCy-3, was synthesized at AFRL with a reported melting point of 391.3 ± 0.1 K, heat of melting of 74 ± 2 J/g, and purity of 99.21 ± 0.04%.[27] Scheme 1 shows the chemical structures for BADCy, SiMCy, ESR-255, and SiCy-3.

Scheme 1. Chemical structures of the di(cyanate esters), BADCy and SiMCy, and the tri(cyanate esters), ESR-255 and SiCy-3.

BADCy

ESR-255
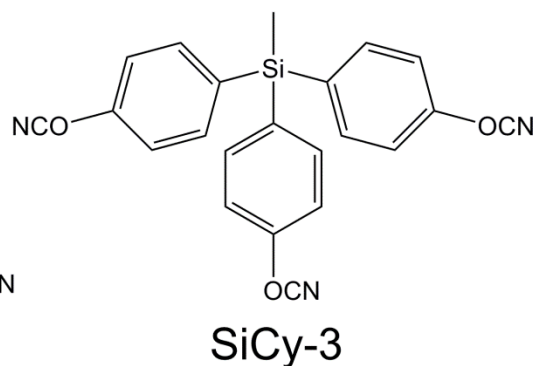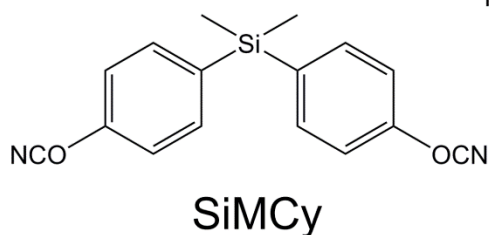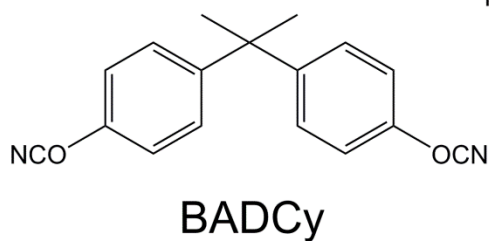
SiMCy

SiCy-3

Crystal Structure Determination. The crystal structures of BADCy,[38,39] SiMCy,[28] and SiCy-3[27] have been previously published. Of the two reports, one structure of BADCy is available in the Cambridge Structural Database (room temperature, presumed 298 K, Refcode: TACHAG[39]) while the other is only available in printed form.[38] The structures for SiMCy (298 K, Refcode: YERHAF) and SiCy-3 (173 K, Refcode: WAGWEJ00) are also available from the Cambridge Structural Database.

For this work, the crystal structure of ESR-255 was collected at room temperature (298 K) using a Bruker ApexII CCD instrument with Mo K_α ($\lambda = 0.71073$ Å) radiation. The data set was were reduced using SAINT,[40] and an empirical absorption correction was applied using SADABS.[41] Structure solution and refinement were conducted using SHELXL-2008 and SHELXL-2014, respectively.[41] All non-hydrogen atoms refined anisotropically. There is minor

disorder with one of the nitrogen atoms in a cyanate ester group, most likely due to librational motion. A table of crystallographic information is located in Supporting Information.

Physical Properties. Analysis of the melting points, enthalpies of fusion, heat capacity, and purity were carried out using a TA Instruments Q200 differential scanning calorimeter (DSC) under 50 mL / min. flowing N_2. Von't Hoff analysis was carried out using the TA Instruments Universal Analysis software package. Because of the reactivity of the compounds under study, the heating rate chosen was based on a compromise between the need to avoid *in-situ* cure (which requires a higher heating rate), and the desire to obtain the best von't Hoff analysis possible (which typically requires a very slow heating rate). The heating rate chosen was 5 K / min. over a range from 313 K to 403 K for von't Hoff analysis, including melting point and enthalpy of fusion measurements.

For high-precision heat capacity measurements, a custom DSC measurement method that has previously been utilized with success in our laboratory for this purpose was modified to accounts for the specific characteristics of the monomers under study. The detailed procedure is given in Supporting Information. In general, the method involves cycling the samples at two different heating and cooling rates across a given temperature range. Because the DSC signal should vary linearly with ramp rate, a linear regression of the data points at a given temperature of interest as a function of ramp rate provides a means of computing heat capacity (proportional to slope) while simultaneously correcting for the sample baseline (proportional to intercept), in both heating and cooling modes. This method was utilized to measure heat capacity in both the crystalline and molten states. More details are provided in Supporting Information (Section S1).

For heat capacity measurements, two sets of cyclic DSC measurements were completed in series, one immediately following the other. In the first cycle, designed to maintain the samples in

the crystalline state, samples were equilibrated at 273 K, then heated at 5 K / min to just below the melting point (T_{c1}), followed by cooling to 273 K, an isothermal hold for 5 min., then re-heating to T_{c1} at 10 K / min., and finally, cooling to 273 K at 10 K / min. The use of two different heating and cooling rates allows for simultaneous calculation of the sample baseline as well as the contribution from heat capacity, in both heating and cooling segments. The second cycle was designed to melt the sample and maintain it in the liquid state to the greatest extent practical. It consisted of heating the sample at 5 K / min past its melting point (T_{m1}), then cooling at 5 K / min to a temperature well below 298 K but not so cold as to cause crystallization on cooling (T_{m2}), followed by re-heating to T_{m1} and re-cooling to T_{m2} at 10 K / min, with a final re-heat to 313 K. Note that most samples crystallized and subsequently melted on re-heating to T_{m1}. The values of the various end-point temperatures must be adjusted according to the melting and crystallization characteristics of each material. As an example, for BADCy, which melts at 355 K, T_{c1} = 353 K, T_{m1} = 383 K, and T_{m2} = 193 K. A full listing of end-point temperature values, a detailed explanation of this technique (which measures the difference in heat capacity between molten and crystalline states) and the required analyses are provided in Supporting Information.

Computational methods. The correlations of Lian and Yalkowsky[25] from 2011 and Chickos and Acree[26] from 2003 were used to estimate the entropy of melting for all four compounds of interest. Generally, these were chosen because they represent the most recent versions available. Note that the Yalkowsky approach calculates the entropy of melting at the melting temperature, while the Chickos approach calculates the entropy of melting at 298 K. In order to facilitate comparisons with experimental data at both the melting point and 298 K, heat capacity data were used to estimate the entropy of melting at 298 K (Detailed data is provided in Supporting Information,

Section S3). To provide additional insight, semi-empirical molecular simulations were carried out using the PM3, MNDO, AM1, and RM1 methods,[42,43] implemented in the GAMESS[44,45] quantum chemistry code.

RESULTS AND DISCUSSION

Crystal Structures Analysis. Figures 1-4 show the crystal packing of BADCy, SiMCy, ESR-255, and SiCy-3, respectively. In general, packing is influenced by the π-π stacking of aromatic rings, and the formation of intermolecular O---H and N---H interactions between the -OCN groups and aromatic hydrogen atoms. Critical intermolecular contacts are shown in Figures 1-4 as turquoise dashed lines. Table 1 presents relevant data obtained from the four crystal structures. From this table, it is observed that the di(cyanate esters), BADCy and SiMCy, pack less densely than the tri(cyanate esters), ESR-255 and SiCy-3. Examination of the packing fractions suggests there is a significant structural difference between the carbon and silicon di(cyanate esters), but only a marginal difference between the tri(cyanate esters). The van der Waals surface areas and volumes for BADCy, SiMCy, ESR-255, and SiCy-3 are consistent with expectations; as the number of bulky ligands increases, the surface areas and volumes increase. This trend is also true for the replacement of the central quaternary carbon with silicon, as Si-C bonds are longer than C-C bonds.

The crystal packing in BADCy has been discussed previously by Fyfe,[38] who noted the formation of a network of close contacts between neighboring cyanate ester groups. However, other investigations of the crystal structure of BADCy have contested that such a network of close contacts exists.[39] This discrepancy is presumably due to the different authors' definition of close contacts. Both reports of BADCy are actually the same, albeit Fyfe *et al*. is in $P2_1/a$ while Davies

10

et al. is in $P2_1/c$. The former is presented in a non-standard setting and can be changed to the latter via the matrix transformation. The crystal packing of SiMCy has also been discussed previously, with a differing network of close contacts identified.[29] These contacts join dimers of SiMCy into ribbons, with each dimer formed by close contact of -OCN groups on aromatic rings stacked in an anti-parallel fashion. The result is a herringbone pattern.

In both ESR-255 and its silicon-containing counterpart SiCy-3, dimers are formed by N---H close contacts that join two molecules (each of which have a "twisted T" shape with aromatic rings in approximately mutually perpendicular planes) into an "H-like" configuration. Additional N---H close contacts then form a pair of interlocked helices. Interestingly, both ESR-255 and SiCy-3 have similar packing patterns. This is partially explained by the fact that both crystal structures are found in centrosymmetric space groups: $P2_1/c$ for ESR-255 and P-1 for SiCy-3. It is therefore not surprising that the enthalpies of melting of ESR-255 and SiCy-3 are quite similar. Even for BADCy and SiMCy, the difference in the enthalpy of melting is only around 3.5% (see Table 2). These effects could change the melting points of the compounds by not more than approximately 10 K. To better compare the differences in crystal structures, Figures 5 and 6 show unit cell comparisons of BADCy v. SiMCy and ESR-255 v. SiCy-3.
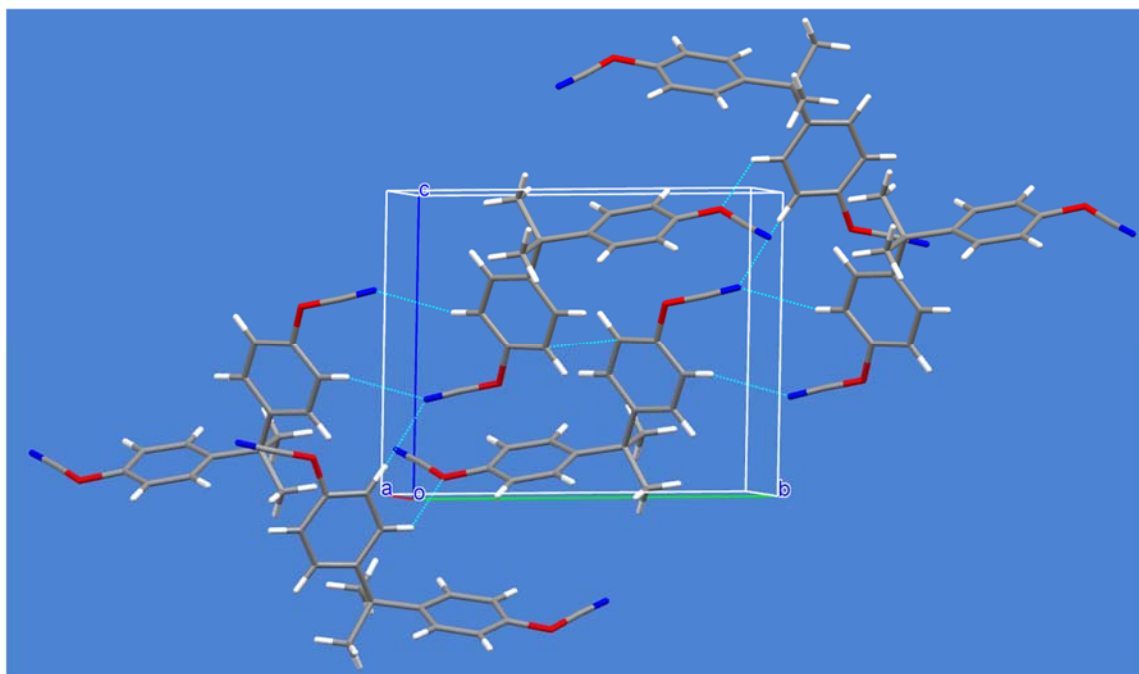
Figure 1. Crystal packing in the unit cell of BADCy, viewed along the *a* direction, exhibiting N--
-H, O---H, and π-π intermolecular interactions shown as turquoise dashed lines. Other colors
represent carbon (grey), hydrogen (white), nitrogen (blue), and oxygen (red).
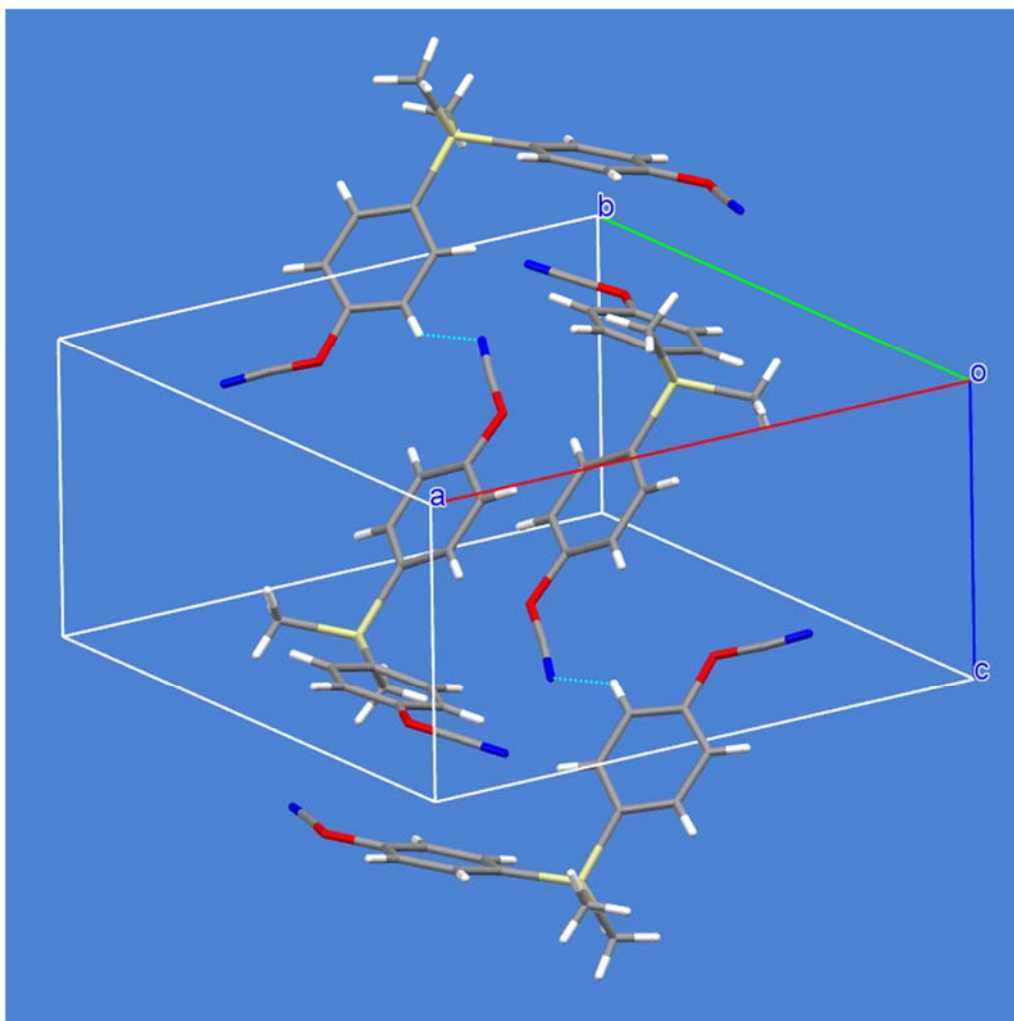
Figure 2. Crystal packing in the unit cell of SiMCy. Close interactions include N---H contacts between the cyanate ester and an aromatic hydrogen atom (shown as turquoise dashed lines), as well as π-π interactions between the phenyl rings (not shown for clarity). Other colors represent carbon (grey), hydrogen (white), nitrogen (blue), oxygen (red), and silicon (yellow).
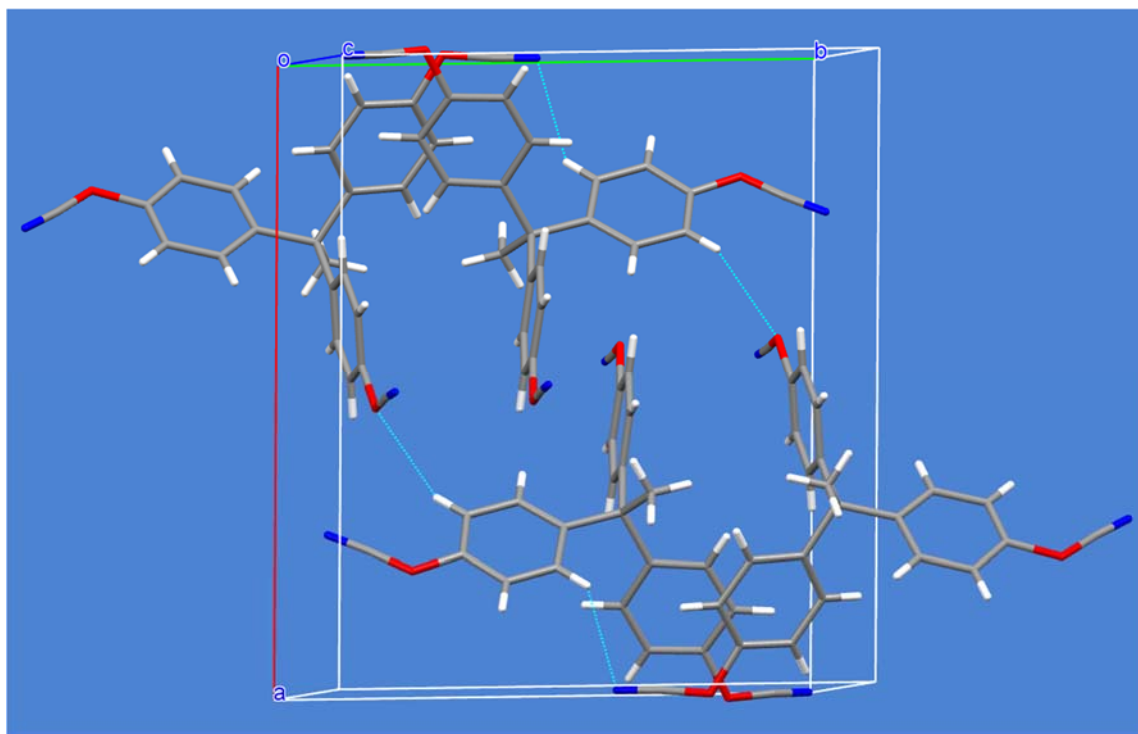
Figure 3. Crystal packing in ESR-255 viewed along the *c* axis. N---H and O---H close contacts shown as turquoise dashed lines, generally along the *a* direction, form pairs. An interlocking helix pattern can be observed along the *c* direction. Strong π-π interactions are not present in this structure. Other colors represent carbon (grey), hydrogen (white), nitrogen (blue), and oxygen (red).
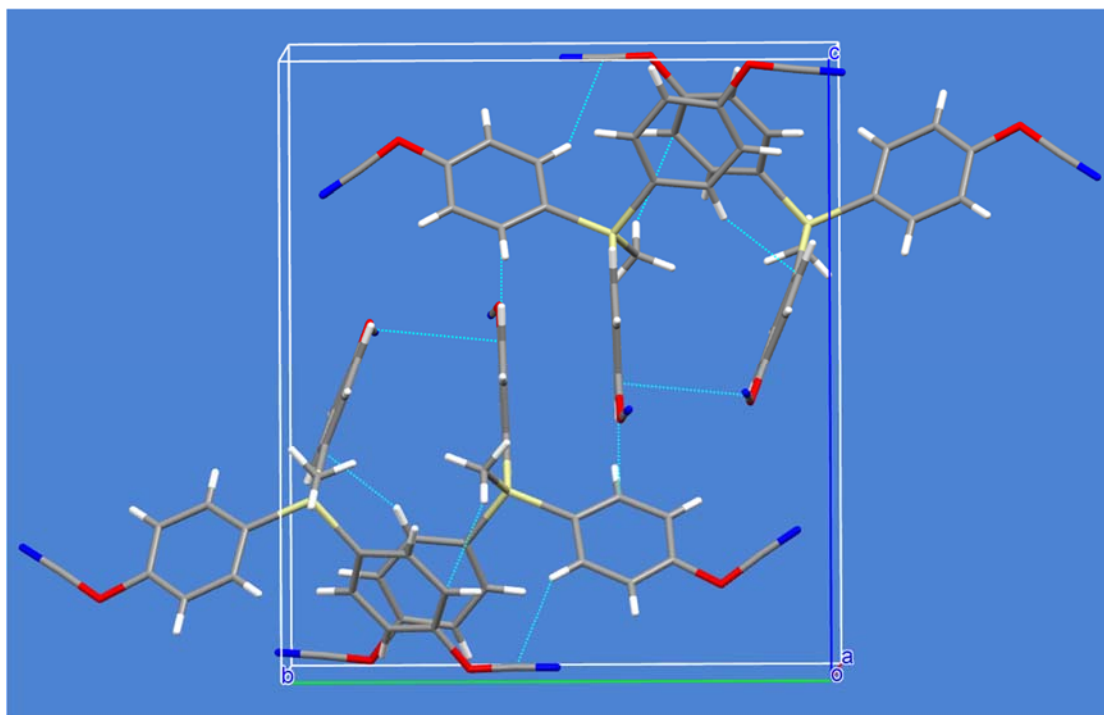
Figure 4. Crystal packing in the unit cell of SiCy-3, viewed along the crystallographic *a* direction. As in ESR-255, N---H close contacts along the *c*-axis combine with additional N---H close contacts along the *b*-direction to form interlocking helices. Intermolecular contacts are shown as turquoise dashed lines. Other colors represent carbon (grey), hydrogen (white), nitrogen (blue), and oxygen (red).
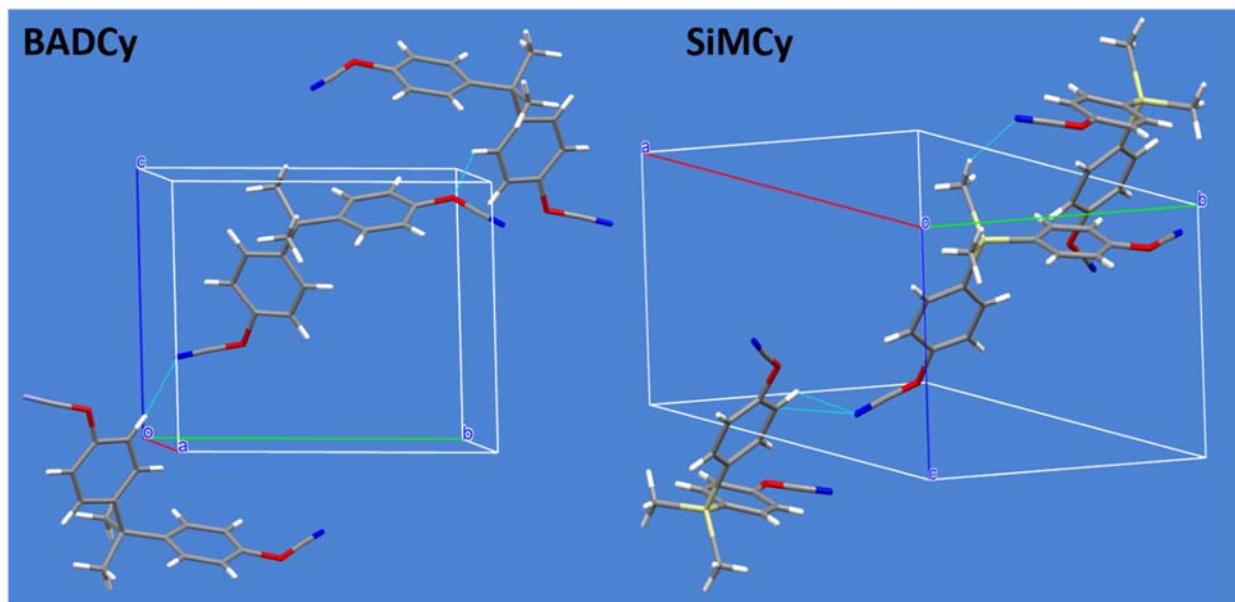
Figure 5. A comparison between BADCy and SiMCy maintaining the relative orientation of the central molecules in the unit cell. Note the clear differences in intermolecular interactions (shown in turquoise) and packing. Other colors represent carbon (grey), hydrogen (white), nitrogen (blue), and oxygen (red).
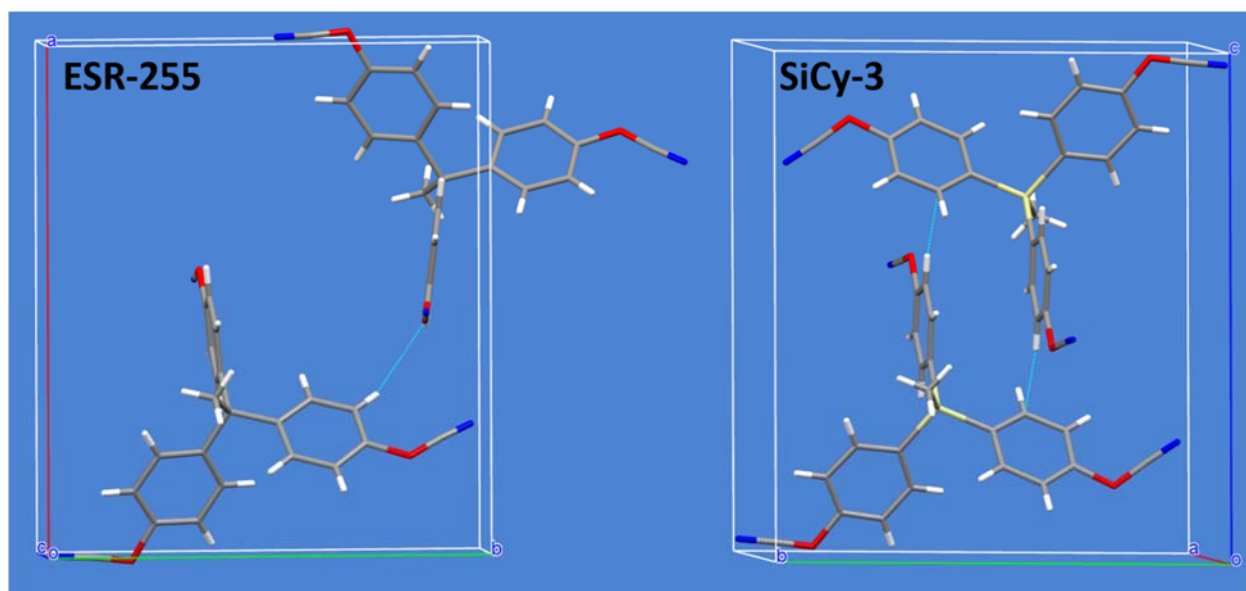
Figure 6. A comparison between ESR-255 and SiCy-3 maintaining the relative orientation of the lower-left molecules in the unit cell. Note the clear differences in intermolecular interactions (shown in turquoise) and packing. Other colors represent carbon (grey), hydrogen (white), nitrogen (blue), and oxygen (red).

Table 1. Relevant data obtained from the crystal structures of BADCy, SiMCy, ESR-255, and SiCy-3.

	Density	Packing fraction	VDW surface ($Å^2$)	VDW volume ($Å^3$)
BADCy[39]	1.276	68.3	287.55	238.55
SiMCy[28]	1.259	66.8	300.78	250.54
ESR-255	1.341	68.6	373.40	317.90
SiCy-3[27]	1.332	68.5	391.39	330.34

Thermodynamic Analysis via DSC. According to Table 2, the equilibrium melting temperature of BADCy is ~22 K higher than that of SiMCy, whereas the melting points of ESR-255 and SiCy-3 differ by less than 2 K. Despite the similarity of these compounds, the substitution of a silicon atom for a carbon atom in the difunctional cyanate ester changes the melting point by ten times as much (and in the opposite fashion) compared to the trifunctional cyanate ester. Figure 7 shows the DSC for the four compounds. Although there may be a stronger network of close contacts in BADCy, the resultant change in the enthalpy of melting is not sufficient to explain the magnitude of the difference alone (although it does make an important contribution). For the difunctional cyanate esters, there is also a significant difference in the entropy of melting, which is not present

17

in the analogous trifunctional cyanate esters. Complete DSC melting point results are provided in Supporting Information, Section S2.
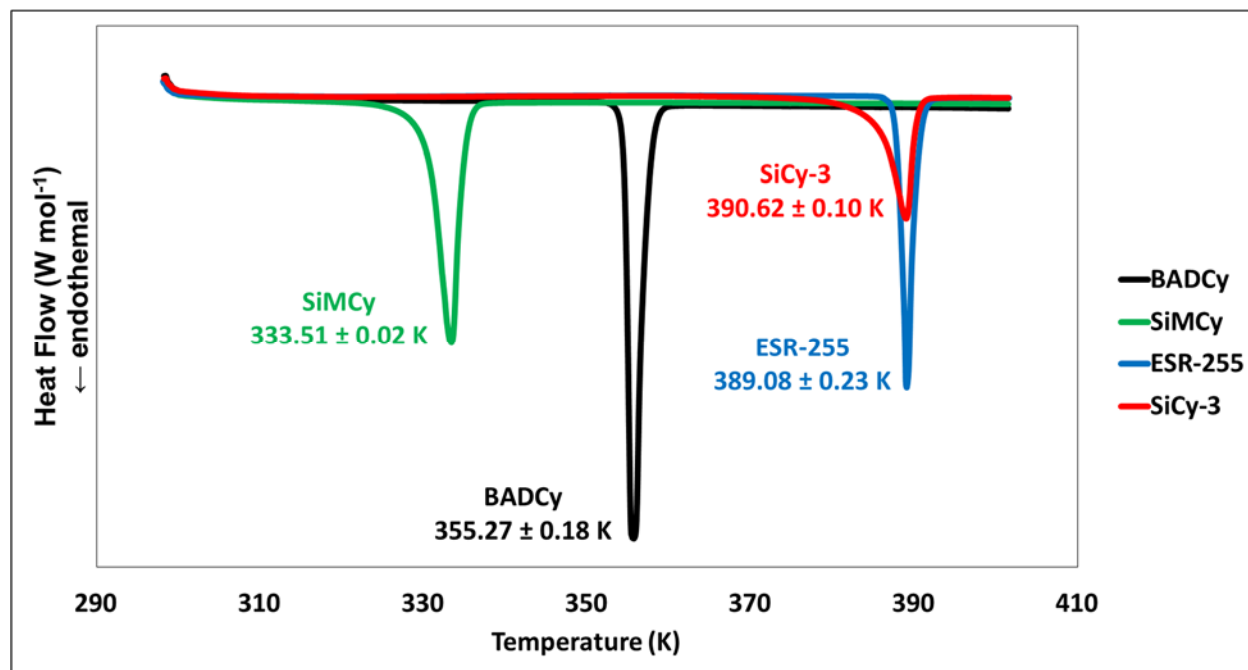
Figure 7. Experimental DSC plots for BADCy, SiMCy, ESR-255, and SiCy-3.

Table 2. Experimental characteristics of cyanate ester crystals determined by DSC

Monomer	T_m^0 (K)	$\Delta H_m^0 \text{-} T_m$ (J mol^{-1})	$\Delta S_m^0 \text{-} T_m$ (J mol^{-1} K^{-1})	Purity (%)
BADCy	355.27 ± 0.18	28.42 ± 0.53	80.0 ± 1.4	99.76 ± 0.09
SiMCy	333.51 ± 0.02	27.38 ± 0.19	82.1 ± 0.6	98.05 ± 0.26
ESR-255	389.08 ± 0.23	29.19 ± 0.74	75.0 ± 1.9	99.54 ± 0.07
SiCy-3	390.62 ± 0.10	29.22 ± 0.29	74.8 ± 0.8	96.22 ± 0.31

Uncertainties are equal to the computed 95% confidence interval using Student's t-distribution. Individual measurements and uncertainties based on Montgomery's range method are provided in Supporting Information, Section S2.

Empirical Calculations. In order to better understand the origins of differences in the entropy of melting of the cyanate ester monomers, two key empirical models were investigated. The Chickos model[26] for the entropy of melting is a group contribution based approach. While it does not offer fundamental information about the causes of entropy changes, it does allow for a potential identification of the specific effects due to the various chemical groups present, and enables the differences seen in the cyanate ester monomers to be put into the context of the whole of the available data for analogous compounds.

The calculations underlying the Chickos model are displayed in Table 3. This table shows each type of chemical group present in the four compounds BADCy, SiMCy, ESR-255, and SiCy-3, listed by row. For each row, the contribution per group is provided in the second colum, followed by the number of such groups present per molecule for each molecule. For example, each nitrile group (model code A56) contributes 17.7 J mol^{-1} K^{-1} to the entropy of melting. For BADCy and SiMCy, there are two such groups per molecule, contributing 2 x 17.7, or 35.4 J mol^{-1} K^{-1} to the entropy of melting For ESR-255 and SiCy-3, there are three such groups, contributing a total of 3 x 17.7, or 53.1 J mol^{-1} K^{-1} to the entropy of melting. Adding together the contributions from each row (some of which are negative) results in the total predicted entropy of melting, shown in comparison with the experimentally observed values, at the bottom of the table. According to the model, the substitution of a quaternary Si atom for a quaternary C atom should increase the entropy of melting at 298 K by approximately 8 J / mol K (based on the different contribution values for groups A4 and A109 as listed in Table 3). For the difunctional cyanate esters, the predicted entropy values as a whole are reasonably close to those observed experimentally, particularly given that the claimed accuracy of the model is around 15 J/mol K. Moreover, the

entropy of melting for SiMCy is 12 ± 3 J/mol K higher than for BADCy, roughly in line with the model prediction.

For the trifunctional monomers, however, the model predictions are inaccurate both in terms of the expected magnitude of the entropy of melting as well as the effect of silicon substitution. Despite a fairly high uncertainty in the observed entropy of melting at 298 K for ESR-255 (due to uncertainties in heat capacity measurements), the entropy of melting is much lower than expected for the trifunctional monomers, and silicon substitution has little effect. Indeed, the trifunctional monomers, containing substantially more atoms than the difunctional monomers, would be expected to have a higher entropy of melting, but even at their respective melting temperatures, the entropies of melting for the trifunctional monomers are lower than those of the difunctional monomers.

Table 3. Application of the Chickos model for entropy of melting to cyanate ester monomers

Group Type	Contribution ($J \, mol^{-1} \, K^{-1}$)	BADCy	SiMCy	ESR-255	SiCy-3
--CH3 (A1)	17.6	2	2	1	1
>C< (A4)	-34.8	1	0	1	0
Nitrile (A56)	17.7	2	2	3	3
Ether (A32)	4.71	2	2	3	3
=CH (A10)	7.4	8	8	12	12
=C- (A11)	-9.6	2	2	3	3
=C- (A12)	-7.5	2	2	3	3
>Si< (A109)	-27.1	0	1	0	1
Total (J/mol K)		70.2	77.9	87.5	95.2
Experimental Adjusted to 298 K (J / mol K)		69.2 ± 3.0	81.1 ± 1.2	50.4 ± 14.1	54.9 ± 3.2

In contrast to the Chickos model, the approach followed by Yalkowsky[25] provides specific fundamental insights into the mechanisms likely to affect the entropy of melting of a small

molecule, at the expense of empirical predictive power. Table 4 summarizes the calculations used in following the Yalkowsky approach. The calculation of the predicted entropy of melting may be obtained from the tabulated data in a similar manner as described earlier for Table 3, except that in this case, individual contributions from structural features, rather than specific chemical groups, are used. Additionally, there is a hierarchy of features. The listed features "SP3", "SP2", "RING", and "Constant" contribute to the parameter τ, which together with the parameters σ and ε, determine the predicted entropy of melting. For instance, in SiMCy, 3 "SP3" features contribute +1 each to τ, two "RING" features add 0.5 each to τ, and the "Constant" adds -1 to τ. τ then has a total value of 3. The contribution from τ is then 3 x 7.4, or 22.2 J mol^{-1} K^{-1}, which is added to the contributions from σ and ε to compute the total predicted entropy of melting.

One issue with this approach is that the effect of substitution of silicon atoms for carbon atoms is not explicitly considered. However, due to the fundamental principles involved, it is straightforward to account for the silicon atom while remaining within the intended spirit of the model. In particular, the model involves counting the number of atoms providing conformational flexibility, using the rule that sp^3 atoms contribute whereas sp^2 atoms do not. Because the quaternary silicon atom would be expected to contribute at least as much conformational flexibility as the quaternary sp^3 carbon, it is clear that it should contribute to the count of "flexible" atoms. Moreover, because the method for determining the anisotropy factor relies on counting groups of planar atoms, and because the bond angles around the silicon atom will be far from planar, the presence of the silicon atom should not affect the anisotropy parameter. Finally, because the symmetry parameter is defined to be one "1" for all molecules containing one or more "flexible" atoms, the substation of the quaternary silicon atom will not change the symmetry parameter.

Table 4. Application of the Yalkowsky model for entropy of melting to cyanate ester monomers

Parameter	Contribution (J mol^{-1} K^{-1})	BADCy	SiMCy	ESR-255	SiCy-3
σ	50 – 19.1 log σ	1	1	1	1
τ	+7.4 τ	3	3	4.5	4.5
SP3	+1 (to τ)	3	3	4	4
SP2	+0.5 (to τ)	0	0	0	0
RING	+0.5 (to τ)	2	2	3	3
Constant	+1 (to τ)	-1	-1	-1	-1
ε	+19.1 log ε	4	4	6	6
Total (J/mol K)		83.7	83.7	98.2	98.2
Experimental ΔS_m (J / mol K)		80.0 ± 1.4	82.1 ± 0.6	75.0 ± 1.9	74.8 ± 0.8

Like the Chickos model, the Yalkowsky approach does well at predicting the total value of the entropy of melting for the difunctional cyanate esters, but overestimates the entropy of melting for the trifunctional cyanate esters. However, it predicts that the substitution of a quaternary silicon for a quaternary carbon will have no effect. For the dicyanate esters, this prediction is incorrect, although one might argue that the effect is too small to be covered by the model. For the tricyanate esters, the prediction is correct. Thus, both models provide partially correct predictions, and neither appears to be significantly different in terms of reliability. One benefit of the Yalkowsky approach, however, is that the fundamental principles underpinning the model can be evaluated. For instance, the Yalkowsky approach determines the anisotropy parameter by independently summing the contributions from separate rigid rings. For prolate molecules with linearly connected rings, which are arguably the most common type of multi-ring small molecules, this approach is intuitively appealing. For the trifunctional cyanate esters, however, the three rings are not arranged linearly but rather in a star-like pattern. As a result, the anisotropy of the molecule as a whole is quite low. If we consider that the correct anisotropy parameter is more likely to be close to unity, then the predicted entropy would be ~15 J/mol K lower than predicted. This brings the predicted value

much closer to the experimental value, although even with this correction the predicted value remains too high.

Semi-empirical Calculations. One limitation of the empirical models described above is that they rely on heuristic approaches to determine factors such as "flexibility". We have already noted that a closer examination of the underlying principles of the model, particularly in the Yalkowsky approach, can improve the predictive power by, for instance, considering the actual, rather than heuristically determined, anisotropy in molecular shape. While a similar geometric approach can be utilized to check the validity of the symmetry parameter (which in all cases is valid), it is more difficult to check a factor such as "flexibility" by heuristic methods. Qualitatively, however, one would expect the substitution of a quaternary silicon for a quaternary carbon to have a potential impact on "flexibility". For instance, because silicon-carbon bonds are longer than carbon-carbon bonds, the rotational barriers among groups bonded to the silicon atom may be lower than those of the same groups when analogously bonded to a carbon atom.

In order to investigate the degree of correlation between the intramolecular steric interactions and the observed melting points in cyanate ester monomers, internal rotational barriers of a series of cyanate ester monomers were computed using semi-empirical quantum chemical calculations. The specific objective of these calculations was to quantify the rotational steric hindrance between the bulky phenyl groups in the di- and trifunctional cyanate esters, BADCy, SiMCy, ESR-255, and SiCy-3, in order to explore the notion that the internal torsional energy barriers around phenyl groups affect the thermal properties of the monomers. For this purpose, calculations of the structures and internal rotation barriers of di- and trifunctional cyanate esters

were performed using the semi-empirical methods: PM3, MNDO, AM1, and RM1[42,43] implemented in the GAMESS[44,45] quantum chemistry code.

To validate the semi-empirical methods, the geometries of the four monomers were fully optimized and compared with the geometries from X-ray crystal structure[29,38,46] measurements. The bond lengths of primary interest are those of the central atom (C1 in BADCy and ESR-255; Si1 in SiMCy and SiCy-3) because they determine how close the attached phenyl groups approach each other. The results are summarized in Table 5, which also includes the predicted geometry of BADCy from molecular density functional theory (DFT) calculations at the B3LYP/6-311G(d,p) level as an additional point of comparison. In general, all of the calculated bond lengths agree reasonably well with experiment. For BADCy, AM1 and RM1 have the largest errors relative to experiment. For example, the predicted C1-C4 bond length is too short by 0.05 angstroms. PM3 and MNDO are slightly better than AM1/RM1, with errors in bond lengths of at most 0.04 Å. Not surprisingly, DFT provides the most accurate bond lengths, differing from experiment by less than 0.02 Å.

The accuracy of the semi-empirical methods for the bond lengths of the tri-functional ESR-255 monomer is similar to that for BADCy, with the PM3 and MNDO (AM1 and RM1) predictions differing from the experimental values by 0.01 − 0.02 (0.02–0.03) Å. For the silicon-containing monomers SiMCy and SiCy-3, however, the accuracies of the semi-empirical methods are more sharply delineated. In particular, the PM3 Si-C bond lengths are within 0.04 Å of the experimental values, whereas MNDO underestimates the Si-C bond lengths by 0.04 − 0.07 Å. AM1 and RM1 likewise perform poorly on the silicon-containing monomers, with Si-C bond lengths underestimated by 0.03 to 0.11 Å. Therefore, the PM3 method was selected for calculations of internal rotational barriers due to its uniformly accurate prediction of the central C-C and Si-C

bond lengths in the four cyanate ester monomers. In general, semiempirical methods such as PM3 are unsuitable for reliable prediction of properties such as bond dissociation energies, reaction barriers, etc. However, they perform well in the modeling of intramolecular steric effects, in which no chemical bonds are formed or broken. Since the primary objective of the computational modeling is simply to determine the extent of correlation between the entropy of melting and the internal rotational barriers, the PM3 method is selected for computation of the latter.

A series of constrained optimizations were performed in order to calculate the maximum internal steric repulsion of neighboring phenyl groups in each of the four monomers. For the di-functional monomers, BADCy and SiMCy, and the tri-functional monomers, ESR-255 and SiCy, two torsional constraints were imposed. Figures 8 and 9 show a schematic representation of molecules and bonds used to define torsions in which M refers to the central atom, C1 in BADCY and ESR-255 and Si1 in SiMCy and SiCy. The dihedral angle ϕ defined by atoms C8-C4-C1-C5 in BADCy and ESR-255 (C8-C4-Si1-C5 in SiMCy and SiCy) was held fixed at a value of 180°. In addition, the dihedral angle θ defined by atoms C6-C2-M-C5, in BADCy and SiMCy was held fixed at values ranging from -180° to +180°, in increments of 30°. The remaining $3n$-8 (n = number of atoms) internal degrees of freedom were fully optimized. The energy profiles thus obtained for BADCY and SiMCy as a function of the constrained torsion angle θ are shown in Figures 10a and 10b, respectively, for which the energies are relative to the corresponding fully optimized (unconstrained) geometries.

For BADCy, the maximum steric repulsion occurs at torsion angle of θ =15° with a maximum steric interaction energy of 16.6 kJ/mol. The local maxima at θ = -60° and θ = 120° are presumably an artifact of PM3, because single point DFT energy calculations at the PM3 geometries indicate the θ = -60° and θ = 120° constrained geometries are local minima.[47] In

SiMCy, the maximum steric repulsion occurs at ±90° but with very low energy of 3.6 kJ/mol. Clearly, the longer Si-C2 and Si-C4 bond lengths of approximately 1.88 Å in SiMCy relative to the C1-C2 and C1-C4 bond lengths of 1.55 to 1.56 Å in BADCy cause less steric crowding of the phenyl groups in the former, thus accounting for the dramatically lower steric interaction energies in SiMCy.

In terms of the entropy of melting, the semi-empirical calculations indicate that in the liquid state at the melting temperature, the relative conformation of the two phenyl rings in BADCy is quite likely to be "locked in" (as opposed to rotating freely through any dihedral angle) with the planes containing each ring at around a 90° angle to one another, which is the same as their conformation in the crystalline state. By contrast, in SiMCy, the two phenyl rings are likely to occupy a range of twist angles relative to one another. In thermodynamic terms, there will be a greater number of possible states for SiMCy in the molten state relative to its crystalline state, thus the entropy of melting will be somewhat higher. Due to the fact that the barrier for relative rotation of the rings is still somewhat larger than RT at the melting temperature, one might expect this "extra" conformational freedom in SiMCy to be less than one full degree of freedom, and thus, that the entropy difference would be less than 8.3 J/mol K (the value of the universal gas constant), as observed experimentally.

A similar analysis was made for the trifunctional monomers ESR-255 and SiCy-3, which is shown in Fig 9. In ESR-255, the presence of a third phenyl group increases the steric repulsion energy relative to BADCy in two regions, $\theta = -120°$ and $\theta = 60°$, with internal rotation barriers of 21.3 kJ/mol and 19.7 kJ/mol, respectively. As shown in Figure 11b, the steric interaction energy profile of SiCy-3 is nearly identical to that of SiMCy (see Figure 10b.) The local energy maxima

occur at the same values of the constraint angle θ (±90°). In the former, the maximum steric

repulsion energy of 3.3 kJ/mol is slightly less than in SiMCy (3.6 kJ/mol).

For a better understanding of the repulsion energy contribution of the third phenyl group

to the monomers, a third torsion is applied to the tri-functional monomers ESR-255 and SiCy-3.

In both cases the dihedral angles ϕ and θ were fixed to 180° and the third dihedral angle, θ', defined

by atoms C5-M-C3-C9 (see Fig 7), was held fixed at values ranging from -180º to +180º, in

increments of $\theta = 30°$. The energy profiles thus obtained as a function of the constrained torsion

angle θ' are shown in Figure 12, for which the energies are relative to the geometries of ESR-255

and SiCy-3 in which ϕ and θ are fixed at 180º but θ' is fully optimized. In ESR-255, the internal

rotation barriers of the third phenyl ring are reduced relative to the second phenyl ring (see Figure

11a.) The maximum steric interaction energy of approximately 13 kJ/mol occurs at θ' = -180, 0,

and +180; i.e., where all three phenyl groups are aligned with the C1-methyl bond. In contrast, the

internal rotation energy profile of the third phenyl group in the silicon analogue SiCy-3, shown in

Figure 12b, is virtually identical to the first (Figure 10b) and second (Figure 11b) phenyl rings.

This result suggests that the primary sources of steric interactions of the phenyl groups in SiMCy

and SiCy-3 are the methyl groups.

The semi-empirical analysis of a single molecule therefore indicates additional

conformational freedom in SiCy-3 relative to ESR-255. The entropy of melting would therefore

also be expected to be larger in SiCy-3 relative to ESR-255. Moreover, the entropy of melting

would be expected to be larger in SiCy-3 than in SiMCy, because the three rings can move

relatively independently of each other (compared to only two in SiMCy). These predictions,

however, disagree with the experimental data. An important consideration missing from the

examination of single molecules is that of intermolecular interactions in the liquid state. In the

difunctional cyanate ester molecules, there is little room for "interleaving" of the phenyl rings. Yet, according to the crystal structure data, in the trifunctional cyanate esters, "interleaving" is present. The loss in density needed to prevent such "interleaved" structures would be significantly greater than is typical for melting of organic molecules (10-15%, a value typically seen in cyanate ester monomers as well). The effect of an "interleaved" structure in the liquid state would be to constrain the rotation of the phenyl rings, and therefore to reduce the entropy of melting. Thus, in the case the trifunctional monomers, while the semi-empirical analysis has not definitively identified the cause of the experimentally observed trends, it has been helpful in identifying the most likely explanation.

Table 5. Calculated and experimental bond distances of BADCy, SiMCy, ESR-255, and SiCy-3.[a]

|	Parameter	Exp.	PM3	MNDO	AM1	RM1	DFT
BADCy	C_1-C_2	1.552	1.521	1.546	1.511	1.508	1.542
	C_1-C_3	1.530	1.534	1.562	1.529	1.530	1.548
	C_1-C_4	1.560	1.520	1.546	1.511	1.508	1.542
	C_1-C_5	1.540	1.534	1.562	1.529	1.530	1.548
SiMCy	Si-C_2	1.876	1.851	1.806	1.789	1.787	-
	Si-C_3	1.856	1.897	1.817	1.832	1.832	-
	Si-C_4	1.883	1.851	1.806	1.789	1.787	-
	Si-C_5	1.857	1.897	1.817	1.831	1.833	-
ESR-255	C_1-C_2	1.539	1.525	1.550	1.514	1.509	-
	C_1-C_3	1.539	1.524	1.550	1.514	1.509	-
	C_1-C_4	1.543	1.523	1.550	1.514	1.510	-
	C_1-C_5	1.549	1.539	1.571	1.536	1.534	-
SiCy-3	Si-C_2	1.875	1.854	1.808	1.790	1.787	-
	Si-C_3	1.866	1.854	1.808	1.790	1.786	-
	Si-C_4	1.879	1.854	1.808	1.790	1.786	-
	Si-C_5	1.868	1.902	1.822	1.834	1.834	-

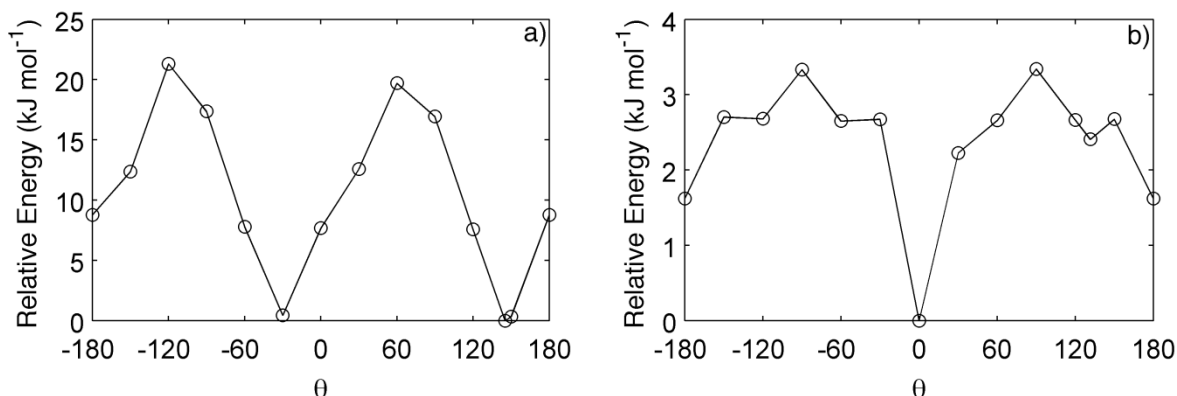[a] See Figure 8 and Figure 9 for the atomic numbering scheme.
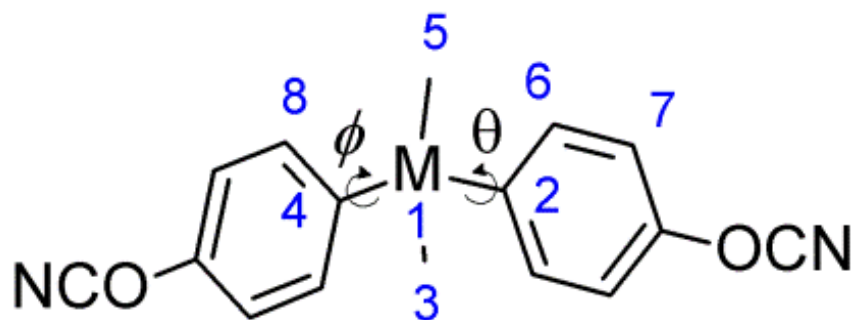
Figure 8. Schematic of the representative molecules and bonds used to define torsions in BADCy and SiMCy.
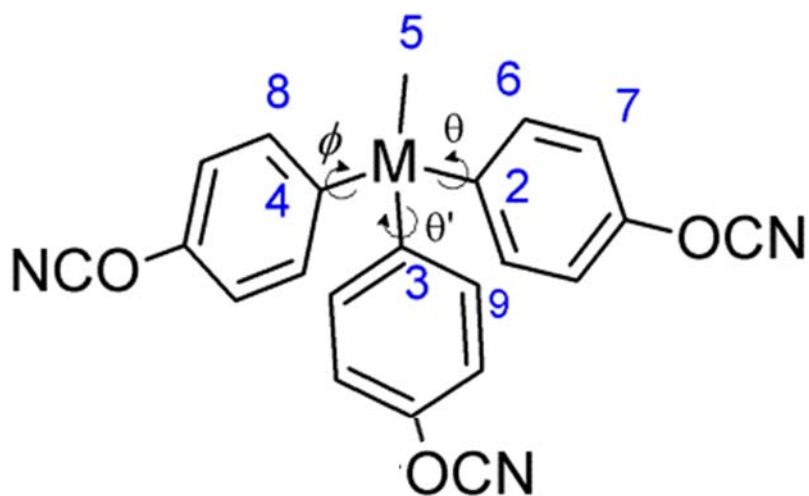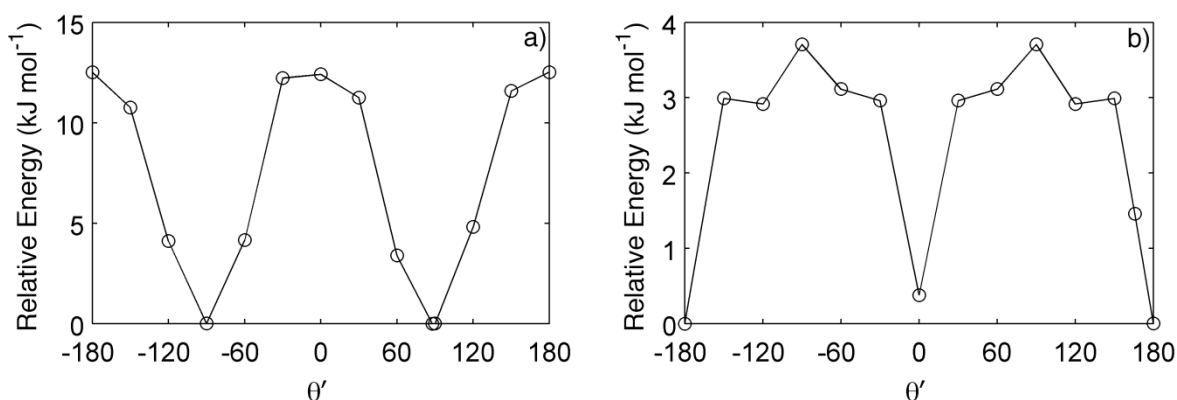

Figure 9. Schematic of the representative molecules and bonds used to define torsions in ESR-255 and SiCy-3.
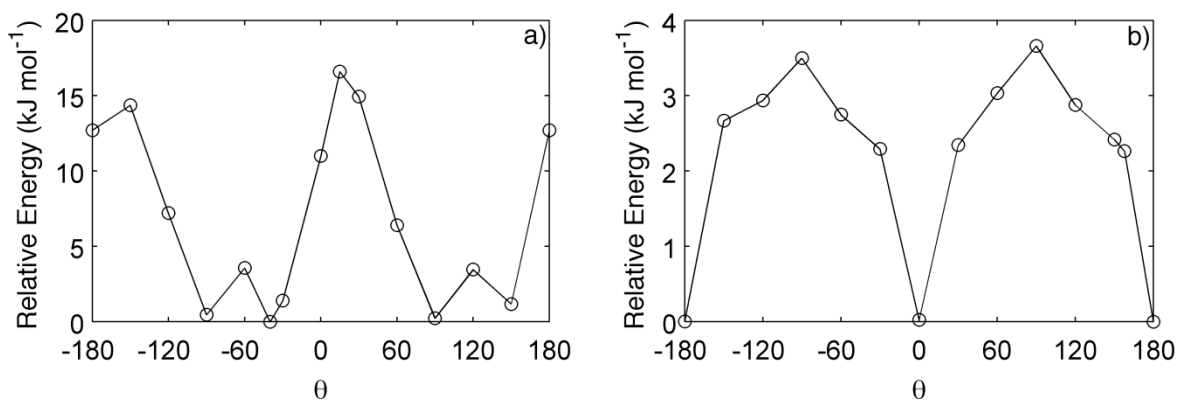
Figure 10. Relative Energy for a) BADCy and b) SiMCy as function of the dihedral angle θ.

Figure 11. Relative Energy for a) ESR-255 and b) SiCy-3 as function of the dihedral angle θ.

Figure 12. Relative Energy for a) ESR-255 and b) SiCy-3 as function of the dihedral angle θ'.

CONCLUSION

Key principles needed for the rational design of thermosetting monomer crystals of, in order to control the melting point, have been elucidated using both theoretical and experimental investigations of cyanate esters. A determination of the thermodynamic properties associated with melting showed that the substitution of silicon for the central quaternary carbon in the di(cyanate ester), 2,2-bis(4-cyanatophenyl)propane, resulted in an increase in the entropy of melting along with a decrease in the enthalpy of melting, leading to a decrease in the melting temperature of 21.8

± 0.2 K. In contrast, the analogous silicon substitution in the tri(cyanate ester), 1,1,1-tris(4-cyanatophenyl)ethane, resulted in no significant changes to the enthalpy and entropy of melting, accompanied by a small increase in the melting point of 1.5 ± 0.3 K. Although both the empirical models of Lian and Yalkowsky, as well as Chickos and Acree, provided reasonable estimates of the entropy of melting of 2,2-bis(4-cyanatophenyl)propane, they successfully predicted only limited effects of silicon substitution, and did not capture the difference in behavior between the di(cyanate esters) and the tri(cyanate esters). Semi-empirical molecular modeling, however, helped to validate an explanation of the mechanism for the increase in the entropy of melting of the silicon-containing di(cyanate ester), while providing insight into the reason for the difference in behavior between the di(cyanate esters) and tri(cyanate esters). Taken together, the results provide enhanced understanding of the ways in which freedom of molecular motions in the liquid state can control the entropy of melting, and can be utilized to guide the development of compounds with optimal melting characteristics for high-performance applications.

SUPPORTING INFORMATION

X-ray data in CIF format is available online free of charge. Detailed description of DSC heat capacity method (S1); DSC raw data for melting (S2) and heat capacity (S3); and crystallographic data table for ESR-255 (S4).

REFERENCES

1. Braga, D. *Chem. Comm.* **2003**, 2751-2754.

2. Desiraju, G. R. *Angew. Chem. Int. Ed.* **1995**, *34*, 2311-2327.

3. Desiraju, G. R. *Crystal Engineering: The Design of Organic Solids*; Elsevier: Amsterdam, The Netherlands, **1989.**

4. Hollingsworth, M. D. *Science* **2002**, *295*, 2410–2413.

5. *Chemistry and Technology of Cyanate Ester Resins*, Hamerton, I., Ed.; Chapman & Hall: London, **1994**.

6. Fang, T.; Shimp, D. A. *Prog. Polym. Sci.* **1995**, *20*, 61-118.

7. Nair, C. P. R.; Mathew, D.; Ninan, K. N. In *New Polymerization Techniques and Synthetic Methodologies*, Abe, A.; Albertsson, A.-C.; Cantow, H. J., Eds.; Springer-Verlag: Berlin, **2001**, *155*, 1-99.

8. Hamerton, I.; Hay, J. N. *High Perform. Polym.* **1998,** *10*, 163-174.

9. Fabian, P.; Haynes, M.; Babcock, H.; Hooker, M. *IEEE Trans. Appl. Supercond.* **2013,** *23*, No. 7700204.

10. Munshi, N. A.; Walsh, J. K.; Hooker, M. W.; Babcock, H. K.; Haight, A. H.; Durso, S. R.; Kawaguchi, A.; Hough, P. *IEEE Trans. Appl. Supercond.* **2013,** *23*, No. 7700104.

11. Wienhold, P. D.; Persons, D. F. *SAMPE J.* **2003,** *39*, 6-17.

12. Laskoski, M.; Dominguez, D. D.; Keller, T. M. *J. Polym. Sci,. Part A: Polym. Chem.* **2006**, *44*, 4559-4565.

13. Yameen, B.; Duran, H.; Best, A.; Jonas, U.; Steinhart, M.; Knoll, W. *Macromol. Chem. Phys.* **2008**, *209*, 1673-1685.

14. Cambrea, L. R.; Davis, M. C.; Groshens, T. J.; Guenthner, A. J.; Lamison, K. R.; Mabry, J. M. *J. Polym. Sci,. Part A: Polym. Chem.* **2010**, *48*, 4547-4554.

15. Goertzen, W. K.; Kessler, M. R. *Composites, Part A* **2007**, *38*, 779-784.

16. Hamerton, I.; Howlin, B. J.; Klewpatinond, P.; Takeda, S. *Macromolecules* **2009**, *42*, 7718-7735.

17. Hwang, H. J.; Li, C. H.; Wang, C. S. *J. Appl. Polym. Sci.* **2005**, *96*, 2079-2089.

18. Crawford, A. O.; Howlin, B. J.; Cavalli, G.; Hamerton, I. *React. Funct. Polym.* **2012**, *72*, 596-605.

19. Lin, C. H.; Hsiao, C. N.; Li, C. H.; Wang, C. S. *J. Polym. Sci,. Part A: Polym. Chem.* **2004**, *42*, 3986-3995.

20. Guenthner, A. J.; Lamison, K. R.; Vij, V.; Reams, J. T.; Yandek, G. R.; Mabry, J. M. *Macromolecules* **2012**, *45*, 211-220.

21. Wells, K. E.; Weatherhead, R. A.; Murigi, F. N.; Nichol, G. S.; Carducci, M. D.; Selby, H. D.; Mash, E. A. *Cryst. Growth Des.* **2012**, *12*, 5056−5068.

22. Gagnon, E.; Halperin, S. D.; Métivaud, V.; Maly, K. E.; Wuest, J. D. *J. Org. Chem.* **2010**, *75*, 399-406.

23. Yu, L. *Acc. Chem. Res.* **2010**, *43*, 1257-1266.

24. Ghiassi, K. B.; Walters, D. T.; Aristov, M. M.; Loewen, N. D.; Berben, L. A.; Rivera, M.; Olmstead, M. M.; Balch, A. L. *Inorg. Chem.* **2015**, *54*, 4565-4573.

25. Lian, B.; Yalkowsky, S. H. *Chemometr. Intell. Lab.* **2011**, *108*, 150–153.

26. Chickos, J. S.; Acree, W. E. *Thermochim. Acta* **2003**, *395*, 59-113.

27. Guenthner, A. J.; Vij, V.; Haddad, T. S.; Reams, J. T.; Lamison, K. R.; Sahagun, C. M.; Ramirez, S. M.; Yandek, G. R.; Suri, S. C.; Mabry, J. M. *J. Polym. Sci., Part A: Polym. Chem.* **2014**, *52*, 767-779.

28. Guenthner, A. J.; Yandek, G. R.; Wright, M. E.; Petteys, B. J.; Quintana, R.; Connor, D.; Gilardi, R. D.; Marchant, D. *Macromolecules* **2006,** *39*, 6046-6053.

29. Hamerton, I.; Emsley, A. N.; Howlin, B. J.; Klewpatinond, P.; Takeda, S. *Polymer* **2003**, *44*, 4839-4852.

30. Hamerton, I.; Howlin, B. J.; Mooring, L.; Stone, C.; Swan, M.; Thompson, S. *Polym. Degrad. Stab.* **2014**, *110*, 435-446.

31. Hamerton, I.; Howlin, B. J.; Klewpatinond, P.; Takeda, S. *Polymer* **2002**, *43*, 5737-5748.

32. Hamerton, I.; Glynn, S.; Hay, J. N.; Pullinger, M. A.; Shaw, S. J. *Polym. Degrad. Stab.* **2012**, *97*, 679-689.

33. Lin, C. H. *Polymer* **2004**, *45*, 7911-7926.

34. Lin, C. H.; Lin, H. T.; Tian, Y. W.; Dai, S. H. A.; Su, W. C. *J. Polym. Sci,. Part A: Polym. Chem.* **2011**, *49*, 4851-4860.

35. Wright, M. E., *Polym. Prepr. (Am. Chem. Soc., Div. Polym. Chem.)* **2004,** *45 (2)*, 294.

36. Shimp, D. A.; Ising, S. J.; Christenson, J. R. In High Temperature Polymers and Their Uses; Society of Plastics Engineers: Cleveland, OH, **1989**; pp. 127-140.

37. Guenthner, A. J.; Davis, M. C.; Ford, M. D.; Reams, J. T.; Groshens, T. J.; Baldwin, L. C.; Lubin, L. M.; Mabry, J. M. *Macromolecules* **2012**, *45*, 9707-9718.

38. Fyfe, C. A.; Niu, J.; Rettig, S. J.; Burlinson, N. E.; Reidsema, C. M.; Wang, D. W.; Poliks, M. *Macromolecules* **1992,** *25*, 6289-6301.

39. Davies, J. M. R.; Hamerton, I.; Jones, J. R.; Povey, D. C.; Barton, J. M. *J. Crystallogr. Spectrosc. Res.* **1990**, *20*, 285-289.

40. *SAINT*; Bruker AXS Inc.: Madison, WI, **2014**.

41. Sheldrick, G. M. *SADABS, SHELXS-2008, SHELXL-2014*; University of Göttingen: Göttingen, Germany, **2014**.

42. Stewart, J. J. P. *J. Comput.-Aided Mol. Des*. **1990**, *4*, 1-105.

43. Rocha, G. B.; Freire, R. O.; Simas, A. M.; Stewart, J. J. P. *J. Comput. Chem*. **2006**, *27*, 1101-1111.

44. Gordon, M. S. Advances in electronic structure theory: GAMESS a decade later, in Theory and Applications of Computational Chemistry: the first forty years; G. F. C. E. Dykstra, K. S. Kim, G. E. Scuseria, Eds.; Elsevier: Amsterdam, **2005**; pp. 1167-1189.

45. Schmidt, K. K. B.; Boatz, J. A.; Elbert, S. T.; Gordon, M. S.; Jensen, J. H.; Koseki, S.; Matsunaga, N.; Nguyen, K. A.; Su, S.; Windus, T. L.; Dupuis, M.; Montgomery, J. A. *J. Comput. Chem.* **1993**, *14*, 1347-1363.

46. Guenthner, A. J.; Reams, J. T.; Lamison, K. R.; Ramirez, S. M.; Swanson, D. D.; Yandek, G. R.; Sahagun, C. M.; Davis, M. C.; Mabry, J. M. *ACS Appl. Matl. Interfaces* **2013**, *5*, 8772-8783.

47. The relative energy values obtained from DFT energy calculations at the PM3 geometries for θ = -90º, -60º, and -30º are 0.92, 2.30, and 10.51 kJ/mol, respectively. For θ = 90º, 120º, and 150º, the corresponding relative energy values are 0, 2.89, and 9.29 kJ/mol, respectively.

TOC Graphic
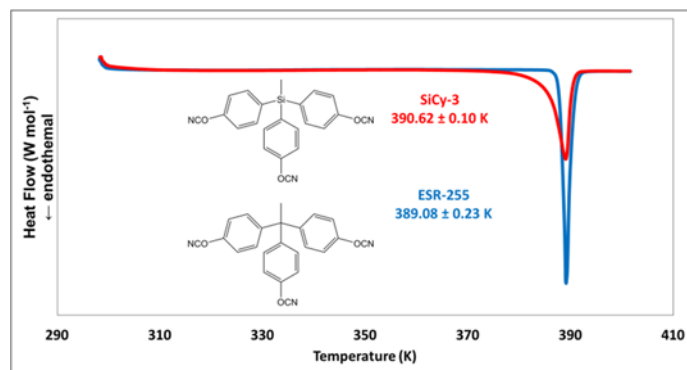
The DSC plots for the cyanate ester monomer, ESR-255, and its silicon counterpart, SiCy-3.

Although structurally different, they are quite thermodynamically similar.

Supporting Information:

Organic Crystal Engineering of Thermosetting Cyanate Ester Monomers: Influence of Structure on Melting Point

Andrew J. Guenthner[1], Sean M. Ramirez[2], Michael D. Ford,[2] Denisse Soto[2], Jerry A. Boatz[1], Kamran B. Ghiassi[1], and Joseph M. Mabry[1]*

[1]Air Force Research Laboratory, Aerospace Systems Directorate, Edwards AFB, CA 93524

[2] ERC Incorporated, Edwards AFB, CA 93524

Author e-mail: andrew.guenthner@us.af.mil

TABLE OF CONTENTS

S1. Details of Heat Capacity Measurement Method

Although seemingly straightforward, the measurement of heat capacities by DSC often requires special considerations in order to ensure sufficient precision and accuracy in the data obtained, typically beyond simple baseline correction methods. These specialized methods often are tailored to the specific materials and measurement objectives involved. In this case, the materials are chemically reactive monomers that have a strong propensity to persist as supercooled liquids. The specific measurement objective is to determine the difference in heat capacity between the crystalline and liquid states in order to estimate the entropy of melting at 298 K in addition to the melting temperature. Because enthalpy and entropy are state variables, the enthalpy and entropy of melting at any temperature may be determined with the aid of Eqs. (S-1) and (S-2), respectively.

$$\Delta H_m(T_1) = \int_{T_1}^{T_m} c_{p,c}(T)\, dT + \Delta H_m(T_m) - \int_{T_1}^{T_m} c_{p,l}(T)\, dT \qquad \text{(S-1)}$$

$$\Delta S_m(T_1) = \int_{T_1}^{T_m} \frac{c_{p,c}}{T}(T)\, dT + \Delta S_m(T_m) - \int_{T_1}^{T_m} \frac{c_{p,l}}{T}(T)\, dT \qquad \text{(S-2)}$$

In the above, H represents enthalpy, S entropy, c_p heat capacity at constant pressure, and T temperature; the subscript c refers to the crystalline state and l to the melt state, while the subscript m refers to a value at the melting temperature and the subscript 1 refers to a single, arbitrarily chosen value. Because the materials involved have melting points not far from 298 K, the heat capacities are well-represented by linear functions of temperature, as assumption that is easily checked by simply examining linear fits of the DSC signal. If $c_{p,c}$ is represented by $a_0 + a_1 T$, and $c_{p,l}$ by $b_0 + b_1 T$, and the result substituted into Eq. S-2, with the integral terms regrouped according to the powers of T associated with the coefficients, the following is obtained:

$$\Delta S_m(T_1) = \Delta S_m(T_m) - \int_{T_1}^{T_m} \frac{b_0 - a_0}{T}\, dT - \int_{T_1}^{T_m} (b_1 - a_1)\, dT \qquad \text{(S-3)}$$

Because the coefficient of the *a* and *b* terms are constants, the integral terms may be evaluated directly, resulting in:

$$\Delta S_m(T_1) = \Delta S_m(T_m) - (b_0 - a_0)(\ln T_m - \ln T_1) - (b_1 - a_1)(T_m - T_1) \qquad \text{(S-4)}$$

According to Eq. (S-4), only the differences between the slopes and intercepets of the linear representations of the heat capacities need to be measured. In a DSC experiment, the output signal may be represented as:

$$y = y_0(T) - mc_p(T)\frac{dT}{dt} \qquad \text{(S-5)}$$

In which *y* represents the measured heat flow signal output from the DSC, the sample mass *m* is constant throughout the experiment in this case, and the heat capacity is a function of temperature, but not of the heating rate *dT/dt*, which can be represented by a constant *Z*. The main issue with DSC measurements is that the baseline heat flow value y_0 tends to depend on the exact sample geometry employed, and tends to differ between heating and cooling segments within the same run. In previous experiments, however, we have observed that y_0 does not appear to depend on the heating rate *Z*. If two different heating rates Z_1 and Z_2 are employed (with negative values representing cooling runs), then as long as the sign of Z_1 and Z_2 does not differ, the difference between the output of the two runs may be represented by

$$y_1 - y_2 = mc_p(T)(Z_1 - Z_2) \qquad \text{(S-6)}$$

The heat capacity as a function of temperature is therefore computable without explicit knowledge of the baseline value if data from two separate heating runs are available across the same temperature range. In order for the approach represented by Eq. (S-6) to be valid, the instrument must be in a steady-state heating or cooling condition to a very good approximation, which in practice means that the runs must begin and end at temperatures well outside the desired data

collection range. Because the heat capacities tend to be very close to linear functions of temperature, this condition is easily verified by examination of the data.

Another important issue arising from DSC measurements in heat capacity is the effect of errors in the measurement of sample mass. These issues are typically avoided by using the largest mass of sample feasible, however, many samples that exist as powders are difficult to pack into small sample pans, and larger sample sizes (in geometric terms) delay the attainment of steady-state heating and cooling conditions, such that the required temperature ranges needed for data collection become unfeasibly large (keep in mind that the monomeric samples are reactive, and thus cannot be heated too far beyond the melting point before chemical reactions ensue, and that high-quality DSC cooling systems have lower temperature limits about 100 K below ambient). If the same sample is utilized in both the crystalline and liquid states, then the error in mass will be identical for both measurements, and when these measurements are subtracted for entropy estimation, the total error will scale simply with the relative error in mass determination. If separate samples are utilized, however, the errors in mass determination will be independently additive, and because the difference in heat capacity is a small fraction of the total, on a relative basis, the error in the difference can become quite large. A similar argument holds true for the use of different heating rates.

It is therefore important to utilize a single sample, tested at different heating and cooling rates, in both crystalline and liquid form, over temperature ranges large enough to achieve steady-state operation over the range of interest (298 K to the melting point), without unduly heating the samples. In order to best satisfy these conditions, we elected to use a standard class of temperature program, tailored to each individual material by adjusting the maximum run temperature to take into account the known melting point of each sample. Because the samples tended to crystallize

on heating from the melt state, we also avoided melting the sample prior to collecting the first "melt" heating, in order to eliminate unnecessary heating of the sample beyond the melting point. (To do so would require an extra heating and cooling loop beyond the melting point.) As a result, data from the first "melt" heating at 5 K / min is not reliable. However, as will become evident, this particular portion of data would not have been reliable for all samples under any circumstances and was therefore not used. As a result, we decided not to sacrifice the reliability of the entire set of "melt" data needlessly by including this extra loop. For less reactive samples in which heating above the melting point is not a detriment to reliability, an extra heating loop to melt the sample and cooling back to the starting point would need to be inserted prior to the "melt" segments of the program.

Table S1-1 lists the steps in the DSC temperature control program utilized to accomplish these objectives. The first column provides a generic description of the segment type (e.g. "heat at 5 K/min."), while the subsequent columns provide the associated starting and ending temperatures selected for each material. For reference, the table also provides the measured melting points. The first portion of the method accomplishes two heating and two cooling runs at two separate rates, over a fairly limited temperature range, in which the material is maintained in its initial crystalline state. Because these ranges are fairly small, the method includes a 5-minute equilibration at 273 K to help maximize the range over which the data is at steady-state. The second part of the method accomplishes melting of the crystals during two heating runs at two separate rates, along with two cooling runs at two separate rates. Generally, the monomers vitrified during cooling, then de-vitrified and re-crystallized during heating. As a result, the available temperature range for analyzing the molten state during heating was not large enough to be useful. Based on the linearity of the data and the absence of any start-up, transition point, or

melting/crystallization effects, specific temperature ranges were chosen over which to carry out heat capacity measurement for each sample. These are listed in Table S1-2.

Table S1-1: DSC Temperature Ramp Program Parameters

Segment	BADCy	SiMCy	ESR-255	SiCy-3
Melting Point	**355.27**	**333.51**	**389.08**	**390.62**
Equilibrate	273.15 K	273.15 K	273.15 K	273.15 K
Heat @ 5K / min	273.15 – 343.15 K	273.15 – 323.15 K	273.15 – 373.15 K	273.15 – 373.15 K
Cool @ 5K / min	343.15K – 273.15 K	323.15 – 273.15 K	373.15 – 273.15 K	373.15 – 273.15 K
Isothermal 5 min	273.15 K	273.15 K	273.15 K	273.15 K
Heat @ 10K / min	273.15 – 343.15 K	273.15 – 323.15 K	273.15 – 373.15 K	273.15 – 373.15 K
Cool @ 10K / min	343.15 – 273.15 K	323.15 – 273.15 K	373.15 – 273.15 K	373.15 – 273.15 K
Heat @ 5K / min	273.15 – 383.15 K	273.15 – 363.15 K	273.15 – 413.15 K	273.15 – 413.15 K
Cool @ 5K / min	383.15 – 193.15 K	363.15 – 193.15 K	413.15 – 223.15 K	413.15 – 223.15 K
Heat @ 10K / min	273.15 – 383.15 K	193.15 – 363.15 K	223.15 – 413.15 K	223.15 – 413.15 K
Cool @ 10K / min	383.15 – 193.15 K	363.15 – 193.15 K	413.15 – 223.15 K	413.15 – 223.15 K

Table S1-2: DSC Temperature Ranges for Heat Capacity Analysis

Intended Material State, Ramp Type	BADCy	SiMCy	ESR-255	SiCy-3
Crystal, Heating	303.15 – 338.15 K	303.15 – 328.15 K (1) 303.15 – 323.15 K (2,3)*	303.15 – 373.15 K	303.15 – 353.15 K
Crystal, Cooling	278.15 – 318.15 K	278.15 – 293.15 K	278.15 – 353.15 K	278.15 – 343.15 K
Melt, Heating	313.15 – 343.15 K	283.15 – 308.15 K	293.15 – 333.15 K	283.15 – 318.15 K
Melt, Cooling	233.15 – 358.15 K (1,3) 288.15 – 358.15 K (2)*	303.15 – 333.15 K	283.15 – 353.15 K	283.15 – 373.15 K

*When values appear in parentheses, they represent variations for individual samples. For instance, for BADCy, crystallization in sample 1 took place at 270 K on cooling the melt in sample 2, but not in samples 1 and 3. The analysis range for melt cooling in sample 2 was therefore shortened to account for this anomaly.

Table S3-1 provides the measured coefficients and difference between crystalline and liquid state values for the heat capacity of each sample measured. For crystalline samples, these coefficients are calculated for both heating and cooling runs, but because data for liquid samples is only available for cooling runs, only the cooling data is utilized for further calculations. Also given is the final tabulation of the net amount to be subtracted from the entropy of melting at the melting temperature in order to estimate the entropy of melting at 298 K. As pointed out

previously, although there are some variations in the absolute values of heat capacity, for most samples, these variations become small when the difference between crystal and liquid state is computed.

In order to illustrate how this method works, we now an example of the data and the analysis for two samples, BADCy #2 and SiCy-3 #1. These two samples were selected at random without preference or exclusion for particularly "good" or "bad" data. Figure S1-1 shows the raw DSC data for BADCy #2, with the various heating and cooling segments color coded. For purposes of fidelity with the raw data format, raw data are disclosed in Centigrade units, while absolute temperatures are used for discussion. Note that the terms "crystal" and "melt" indicate the intended state of the material based on the DSC program, and do not necessarily reflect the actual material state. In fact, the data for the intended crystalline and melt states matches almost exactly during heating above 300 K. The presence of the large exotherm during heating at lower temperatures demonstrates clearly that the sample crystallizes under these conditions. Somewhat surprisingly, despite the multiple crystallization peaks, the heat capacity of the resultant crystalline material exactly matches that of the starting material. On cooling of the melt at 5 K / min, a very large exotherm is present at around 270 K, also indicating crystallization. On cooling below about 235 K, a glass transition is visible, modestly in the crystallized sample, and very clearly in the molten sample. This feature thus helps to confirm that at 10 K / min, the sample remained molten throughout cooling, while during cooling at 5 K / min, the sample crystallizes partly during cooling, with the remaining crystallization taking place on subsequent heating at 10 K / min.
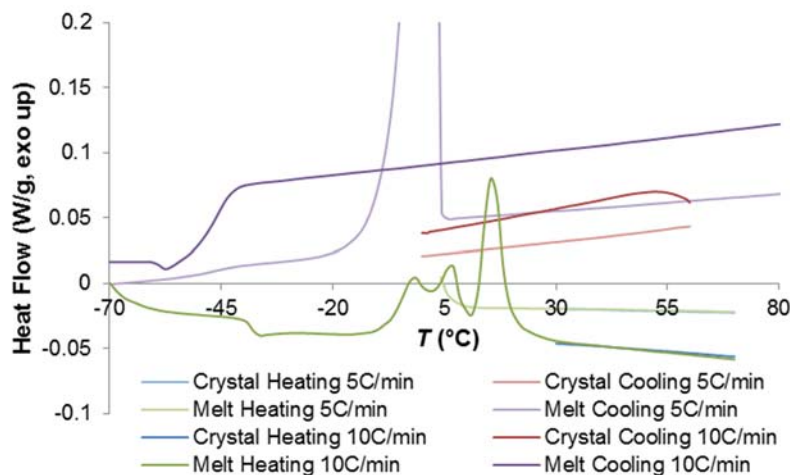
Figure S1-1. DSC traces of BADCy sample #2 during programmed temperature ramps. The terms "crystal" and "melt" refer to the intended sample state. In reality, the sample has partly crystallized during "melt" cooling at 5 °C/min below about 0 °C, is partly crystalline during "melt" heating at 10 °C/min up to around -10 °C, and then fully crystallizes by about 30 °C. Because these issues render "melt" heating data unreliable, the sample was kept in the crystalline state during "melt" heating at 5 K / min also.

In Figure S1-2, only the linear portions of the data, which are useful for analysis of heat capacity, are shown. Again, the crystal and melt data on heating heating coincide because the "melt" sample has either not melted, or it has re-crystallized. Data with a perfect baseline adjustment would show curves at 10 K / min that were twice the magnitude of those at 5 K / min. This condition is close to, but not quite, met. As explained in Section S1, however, one can utilize the difference between these curves to extract the heat capacity (as shown in Figure S1-3), one can also "extrapolate" the curves to zero heating or cooling rate to extract the baseline, as shown in Figure S1-4.
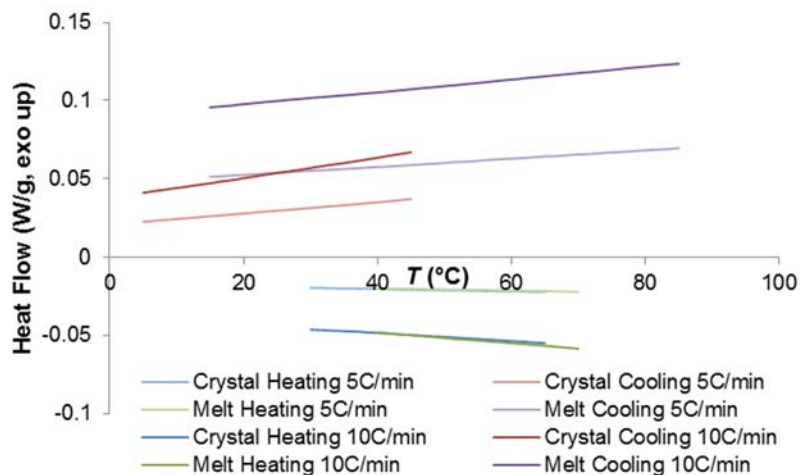
Figure S1-2. DSC traces of BADCy sample #2 during programmed temperature ramps. The terms "crystal" and "melt" refer to the intended sample state. In reality, during the "Melt Heating" portions, the sample is actually in the crystalline state.
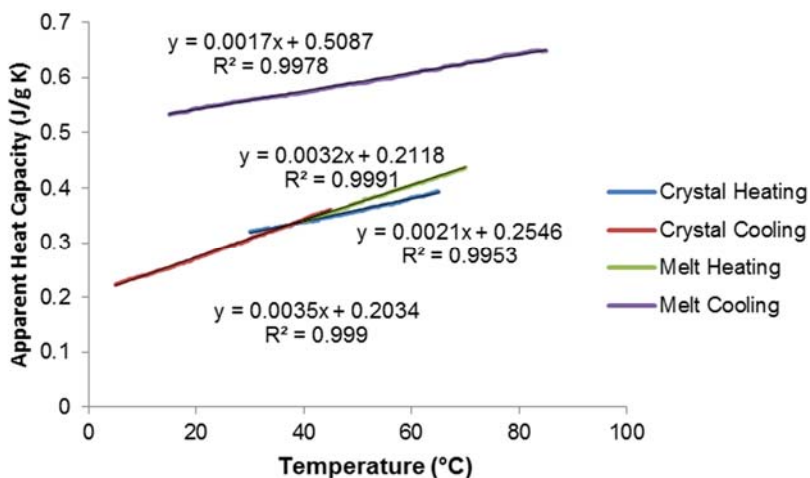

Figure S1-3. Computed apparent heat capacity data from the curves shown in Figure S1-2.
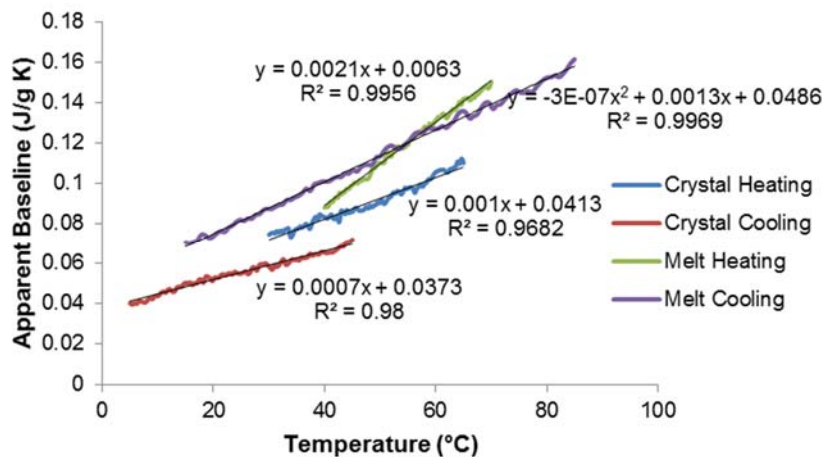
Figure S1-4. Computed baselines from the curves shown in Figure S1-2.

The computed crystalline heat capacity curves in Figure S1-3 are all similar, with the initial heating data being slightly different. Note once again that the sample has re-crystallized for "melt heating", thus the coincidence with the other data for the crystalline sample. In fact, given the variation in thermal history and the possibility of polymorphism, the agreement is surprisingly good. Figure S1-4 confirms that the computed baselines, though similar to one another, do shift slightly during the course of the experiment. The baseline for "melt heating" (sample actually crystalline) seems to fit the pattern least well. This discrepancy may be the only manifestation of the difference between the "not melted" material in the 5 K / min segment, as opposed to the "re-crystallized" material in the 10 K / min segment. Because of the multiple issues identified with heating data, the cooling data was chosen as the basis for heat capacity calculation, and the heating data was ignored (we present it only for completeness). The linear regressions using ordinary least squares of the data in Figure S1-3 confirm that the model of heat capacity as a linear function of temperature is quite appropriate.

10

Figures S1-5 through S1-8 provide the analogs of Figures S1-1 through S1-4 for SiCy-3 sample #1. In the raw DSC scan, the glass transition, re-crystallization, and melting of SiCy-3 are all apparent, as in BADCy. The only difference is that, in the SiCy-3 data, there is actually a linear portion of the curve for the molten state in the 10 K / min "melt heating". In the 5 K / min segment, however, the sample remains in the crystalline state. The algorithm that computes heat capacity therefore fails in this case, producing meaningless data. Because only the cooling data was used for analysis, we did not attempt to correct this issue; we point it out only so that readers will understand the limitations of the particular DSC program we employed.
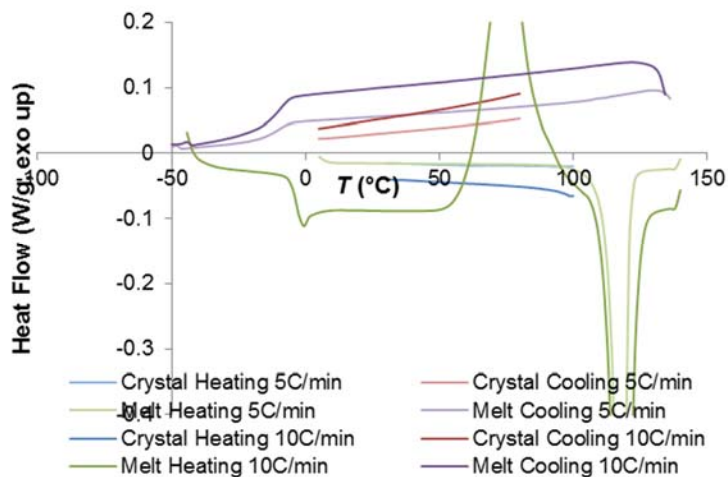
Figure S1-5. Raw DSC data for SiCy-3 sample #1. Note that during the "melt heating" segment, the sample is actually crystalline at the slower heating rate, and that it re-crystallizes at the faster heating rate.
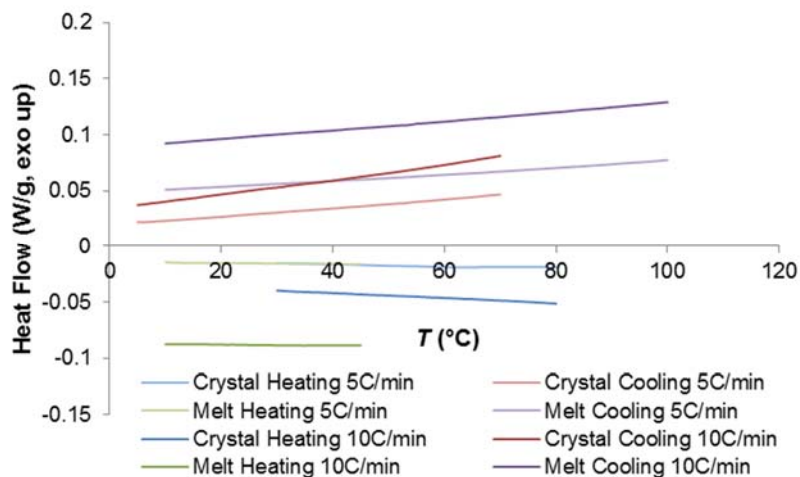
Figure S1-6. Linear portions of the DSC data from Figure S1-5. Note that the sample in the "Melt Heating 5 C / min" segment is actually in the crystalline state.

Figure S1-7. Computed heat capacities for SiCy-3 based on the data in Figure S1-6. Note that the "melt heating" capacity is not computed correctly by the chosen algorithm because the sample was not actually molten during both "melt heating" segments.
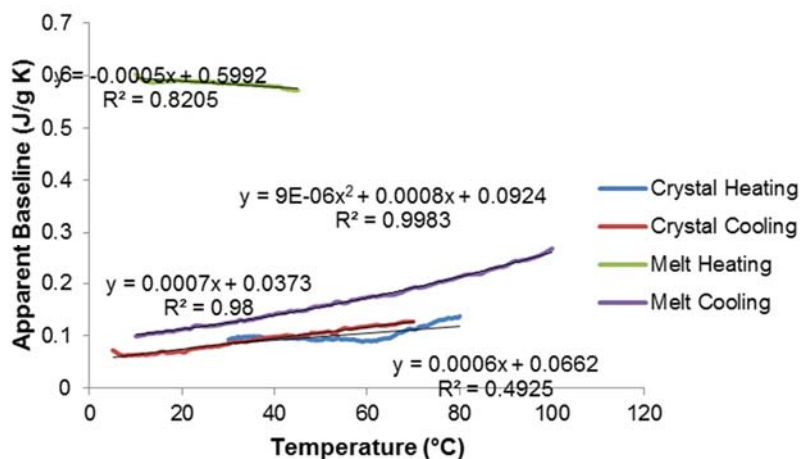
Figure S1-8. Extrapolated baselines based on the data in Figure S1-6. Note that the calculation for the "melt heating" segments is incorrect because the sample was not actually molten during these segments.

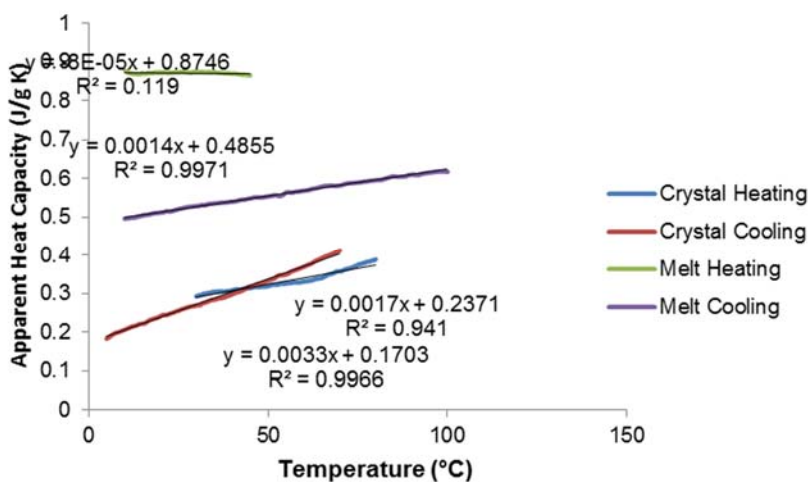Like the BADCy data, the baselines are reasonably close to one another, with a slight difference between heating and cooling. The heat capacities also follow a very similar pattern to BADCy. The crystal heating baseline does show a modest non-linearity due to its nearness to the onset of the wide melting peak. Because we elected not to use heating data, this issue did not affect the results.

As a final point, it must be emphasized that the heat capacity measurements employed were tailored to meet the specific requirements of measuring only the difference in heat capacity between crystal and supercooled molten (above the glass transition) states for purposes of computing the entropy of melting at temperatures other than the equilibrium melting point. The methods were also tailored for maximum reliability when using reactive monomers that could change their chemical composition when heated above the melting point. This highly specific algorithm should not be utilized without modification for other purposes, including

13

measurement of absolute heat capacities, measurement of non-reactive materials, measurement of materials that crystallize readily on cooling, materials that vitrify at temperatures close to the melting point, or other variations.

S2. DSC Melting Point Data

Table S2-1 provides a complete listing of all computed parameters from DSC melting point analysis. The linear baseline integrations, linear baselined peak (uncorrected melting point), corrected melting point estimates, peak area corrections, and purities based on the von't Hoff method were all determined by TA Instruments Universal Analysis software. The standard deviations are based on the Montgomery range method.

Table S2-1. Computed values from the DSC melting experiments.

Monomer	Sample #	T_m (K, uncorrected)	ΔH_m (J mol^{-1}, uncorrected)	Purity	T_m (K, corrected)	ΔH_m (J mol^{-1}, corrected)
BADCy	1	354.56	26.08	99.78	355.24	28.26
BADCy	2	355.69	26.16	99.79	355.22	28.05
BADCy	3	354.51	26.40	99.82	355.14	28.17
BADCy	4	355.61	26.48	99.79	355.24	28.48
BADCy	5	354.59	26.20	99.63	355.53	29.12
SiMCy	1	333.30	25.25	97.72	333.51	27.43
SiMCy	2	333.41	25.55	98.13	333.53	27.46
SiMCy	3	333.41	25.69	98.13	333.48	27.54
SiMCy	4	333.42	25.27	98.28	333.50	27.14
SiMCy	5	333.31	25.33	98.01	333.51	27.35
ESR-255	1	389.12	25.95	99.58	389.07	29.28
ESR-255	2	389.28	25.97	99.45	389.35	29.35
ESR-255	3	389.18	26.25	99.53	389.10	28.79
ESR-255	4	389.08	26.71	99.56	389.02	30.04
ESR-255	5	388.97	26.21	99.58	388.84	28.47
SiCy-3	1	388.79	25.76	96.16	390.58	29.17
SiCy-3	2	388.76	25.73	95.86	390.66	29.19
SiCy-3	3	389.05	25.93	96.25	390.66	29.23
SiCy-3	4	388.93	25.72	96.29	390.70	28.93
SiCy-3	5	389.08	26.35	96.54	390.49	29.58

The raw data generally look good, but do show some points worth noting. For BADCy, in sample 5, the von't Hoff correction appears to produce significant different results (highlighted in blue) from a sample with uncorrected data that appear typical. Such a result may be the consequence of

a disturbance in the raw signal that modestly affected the correction algorithm. The sample-to-sample variability also appears unusually high for ESR-255, particularly for the corrected enthalpies of melting, while the uncorrected enthalpy of melting data show only one outlier (sample 4, noted in blue) Also of concern are the differences in sample purity, whereas BADCy and ESR-255 are quite pure, the silicon-containing samples, particularly SiCy-3, are of lower purity. The potential effect of these issues on the data and inferences drawn were therefore checked.

Because our main concern was with the comparative entropies of melting for all four monomers, we checked the effects of the correction algorithm by computing the equivalent of Table 1 using uncorrected enthalpies of melting. The results are shown in Table S3-2 (note that we retain 4 significant figures for the enthalpy of fusion only to facilitate comparison with Table 2 in the main text).

Table S3-2. Experimental Characteristics of Cyanate Ester Crystals Based on Uncorrected Entnalpies of Melting

Monomer	T_m^0 (K)	$\Delta H_m^0(T_m)$ (kJ mol^{-1})	$\Delta S_m^0(T_m)$ (J mol^{-1} K^{-1})	Purity (%)
BADCy	355.27 ± 0.18	26.26 ± 1.44	73.9 ± 0.6	99.76 ± 0.09
SiMCy	333.51 ± 0.02	25.42 ± 0.47	76.2 ± 0.7	98.05 ± 0.26
ESR-255	389.08 ± 0.23	26.21 ± 1.90	67.4 ± 1.0	99.54 ± 0.07
SiCy-3	390.62 ± 0.10	25.90 ± 0.76	66.3 ± 0.9	96.22 ± 0.31

From Table S3-2, it can clearly be seen that comparatively, there is no change in the pattern among the monomers of the entropy of melting, although, in absolute terms, both enthalpy and entropy of melting decrease. The uncertainties in the entropy of melting are certainly more uniform, however, and the substantially smaller uncertainty for BADCy makes the difference with SiMCy seemingly more significant. These results indicate that while the correction algorithm may be introducing extra uncertainty into the computed parameters, the algorithm does not appear to introduce bias that affects the conclusions.

To check the effects of outliers, we did not resort to specific tests for outliers, given that the data sets have only five samples, and there are only two potential candidates. We simply looked at how the results would change if these samples were excluded. Excluding the outlier in the corrected enthalpy of melting for BADCy changes the average enthalpy of melting (corrected) to 28.24 ± 0.29 J mol^{-1}, the melting point to 355.21 ± 0.06 K, and the entropy of melting (corrected) to 79.5 ± 0.8 J mol^{-1} K^{-1}. These values are not significantly different from those reported in Table 1, and only strengthen the case that the entropy of melting is higher for SiMCy.

S3. DSC Heat Capacity Data

Table S4-1 lists the measured heat capacity coefficients for both crystalline and melt state of all cyanate ester monomers studied. The relevant equations and definitions are provided in Section S1. Also provided are the parametric differences that contribute to the adjustment of the entropy of melting for temperatures other than the equilibrium melting point. Table S3-2 lists the computed adjustments for the entropy of melting at 298 K, along with relevant statistical information in Table S3-3. For purposes of uncertainty computation, we consider the uncertainties in the values of the heat capacity coefficients to be wholly captured in the observed variation in the corrections themselves. Thus, the computed uncertainty reflects the uncertainty in the original entropy of melting measurements at the equilibrium melting point, combined assuming no correlations with the uncertainty in the correction. The large uncertainty for ESR-255 appears to result from unusual values for the molten state heat capacity of one of the samples, most likely from a baseline shift during measurement. As explained in Section S1, these data are derived from only the cooling portions of the DSC program, because the heating portions were more affected by re-crystallization of samples, nonlinearities due to the onset of melting, and greater potential

instability of the baseline during the initial heating segments. We emphasize that these data may

not be reliable for computation of absolute heat capacity values.

Table S3-1. Measured Heat Capacity Parameters

Monomer / Sample	Crystalline State		Molten State	
	a_0 (J g^{-1}K^{-1})	a_1 (J g^{-1}K^{-2})	b_0 (J g^{-1}K^{-1})	b_1 (J g^{-1}K^{-2})
BADCy / 1	-0.788	0.00319	-0.0264	0.00153
BADCy / 2	-0.744	0.00347	0.0523	0.00167
BADCy / 3	-0.682	0.00326	0.0384	0.00177
SiMCy / 1	-1.603	0.00702	0.150	0.00155
SiMCy / 2	-1.513	0.00699	0.216	0.00162
SiMCy / 3	-1.675	0.00702	0.0782	0.00153
ESR-255 / 1	-0.646	0.00355	0.0656	0.00198
ESR-255 / 2	-0.596	0.00332	0.374	0.00129
ESR-255 / 3	-0.513	0.00329	0.348	0.00138
SiCy-3 / 1	-0.738	0.00333	0.108	0.00138
SiCy-3 / 2	-0.702	0.00337	0.165	0.00137
SiCy-3 / 3	-0.651	0.00314	0.180	0.00127

Table S3-2. Heat Capacity at 298 K Computation

Monomer / Sample	Correction Magnitudes		Correction	
	(b_0-a_0) (J/g^{-1}K^{-1})	(b_1-a_1) (J/g^{-1}K^{-2})	ΔS (T$_m^0$-298 K) (J/mol^{-1}K^{-1})	ΔS_m (298 K) (J/mol^{-1}K^{-1})
BADCy / 1	0.762	-0.00167	-10.7	69.3
BADCy / 2	0.796	-0.00180	-10.3	69.7
BADCy / 3	0.720	-0.00149	-11.5	68.5
SiMCy / 1	1.753	-0.00547	-0.9	81.2
SiMCy / 2	1.729	-0.00537	-1.2	80.9
SiMCy / 3	1.753	-0.00549	-0.7	81.4
ESR-255 / 1	0.712	-0.00137	-24.8	50.2
ESR-255 / 2	0.970	-0.00204	-27.8	47.2
ESR-255 / 3	0.862	-0.00191	-21.3	53.7
SiCy-3 / 1	0.846	-0.00194	-19.4	55.4
SiCy-3 / 2	0.867	-0.00200	-19.5	55.3
SiCy-3 / 3	0.831	-0.00187	-20.1	54.1

Table S3-3. Statistical Characteristics of Entropy of Melting at 298 K

Monomer	$(b_0 - a_0)$ $(J/mol^{-1}K^{-1})$	$(b_1 - a_1)$ $(J/mol^{-1}K^{-2})$	ΔS $(T_m{}^0\text{-}298\ K)$ $(J/mol^{-1}K^{-1})$	ΔS_m (298 K) $(J/mol^{-1}K^{-1})$
BADCy	0.759 ± 0.163	0.00165 ± 0.00067	-10.8 ± 2.7	69.2 ± 3.1
SiMCy	1.745 ± 0.058	0.00544 ± 0.00027	-1.0 ± 1.0	81.1 ± 1.2
ESR-255	0.847 ± 0.557	0.00177 ± 0.00153	-24.6 ± 13.9	50.4 ± 14.1
SiCy-3	0.848 ± 0.077	0.00194 ± 0.00030	-19.9 ± 3.1	54.9 ± 3.2

Uncertainties represent 95% confidence intervals using Student's t-distribution

In order to better understand the sources of uncertainty in the model, a brief analysis was conducted, with the results shown in Table 3-4. Because the data can be either positive or negative, the typical coefficient of variation approach is inappropriate. Instead, we use the sample standard deviation as a measure of variance, and then examine the effect on the heat capacity (or difference in heat capacity) value itself, at a temperature that is halfway between 298 K and the approximate average melting point of all samples. This midpoint temperature was about 333 K. Thus, the sample standard deviations of the b coefficients were multiplied by 333 in order to establish a consistent measure of variation for comparison purposes.

Table S3-4. Analysis of Variation in Heat Capacity Parameters

Parameter	a_0 $(J/mol^{-1}K^{-1})$	a_1 $(J/mol^{-1}K^{-2})$	b_0 $(J/mol^{-1}K^{-1})$	b_1 $(J/mol^{-1}K^{-2})$	$(b_0 - a_0)$ $(J/mol^{-1}K^{-1})$	$(b_1 - a_1)$ $(J/mol^{-1}K^{-2})$
BADCy	0.053	0.049	0.042	0.040	0.038	0.052
SiMCy	0.081	0.006	0.069	0.016	0.014	0.021
ESR-255	0.067	0.047	0.171	0.125	0.130	0.118
SiCy-3	0.044	0.041	0.038	0.020	0.018	0.022
Average	0.061	0.036	0.080	0.050	0.050	0.053

A few insights may be gleaned from the analysis shown in Table S3-4. First, the largest variations may be traced to the b coefficients in ESR-255, due to the anomalous values of b coefficients for sample ESR-255 / 1. The most likely root cause that would affect both b coefficients but not the corresponding a coefficients would be a shift in the baseline during measurement. Figures S1-4 and S1-8 do show that the baseline can vary during the course of a single DSC run, if the variation happens between analogous segments run a 5 K / min and 10 K /

min, an error of the type seen for sample ESR-255 / 1 would result. If the anomalous results for ESR-255 (shown in blue) are excluded, then the contributions from all four fitting parameters are similar, with a slightly lower contribution for the first-order (temperature-dependent) term. For the constant terms, the variation in the difference does appear to be substantially lower than the variation in the individual terms, while for the first-order term, the variations are similar. Thus, as expected, the use of the difference terms does eliminate some error, and the use of a single DSC sample, rather than separate runs with separate samples, does have some benefit. Lastly, the actual difference in heat capacity between molten and crystalline states was typically ~ 0.2 J g^{-1} K^{-1}, so the variations in the differences, being about one order of magnitude less, were suitably small. When used to compute relatively small corrections to the entropy of melting, the use of only three samples did make the 95% confidence interval relatively large compared to the magnitude of the correction, however, because the correction itself was small, the overall uncertainty was still reasonable in most cases. A larger number of samples (5-10) would be needed to make the uncertainties in the 298 K melting entropies as small as those at the melting point, but for this particular study, the level of precision provided was sufficient.

S4. Crystallographic Information for ESR-255

Identification code	kbg400
Empirical formula	$C_{23}H_{15}N_3O_3$
Formula weight	381.38
Temperature	296(2) K
Wavelength	0.71073 Å
Crystal system	Monoclinic
Space group	$P2_1/c$
Unit cell dimensions	$a = 15.8072(14)$ Å $\alpha = 90°$.
	$b = 13.5288(12)$ Å $\beta = 97.8393(17)°$.
	$c = 8.9192(8)$ Å $\gamma = 90°$.
Volume	1889.6(3) Å^3
Z	4
Density (calculated)	1.341 Mg/m^3
Absorption coefficient	0.091 mm^{-1}
$F(000)$	792
Crystal size	0.390 x 0.280 x 0.130 mm^3
Crystal color and habit	colourless block
Diffractometer	Bruker ApexII
Theta range for data collection	1.989 to 28.697°.
Index ranges	$-21<=h<=21, -18<=k<=18, -12<=l<=12$
Reflections collected	26603
Independent reflections	4872 [R(int) = 0.0223]
Observed reflections ($I > 2$sigma(I))	3630
Completeness to theta = 25.242°	100.0 %
Absorption correction	Empirical
Max. and min. transmission	0.9631 and 0.8406
Solution method	SHELXS (Sheldrick, 2008)
Refinement method	SHELXL-2014/7 (Sheldrick, 2014)
Data / restraints / parameters	4872 / 0 / 272
Goodness-of-fit on F^2	1.037
Final R indices [I>2sigma(I)]	$R_1 = 0.0491, wR_2 = 0.1292$
R indices (all data)	$R_1 = 0.0657, wR_2 = 0.1414$
Extinction coefficient	n/a

Largest diff. peak and hole   0.262 and -0.231 e Å^{-3}